Title
External Mass Injection to Reduce Energetic Ion Production in the Discharge Plume of High Current Hollow Cathodes

Permalink
https://escholarship.org/uc/item/2kt8s39z

Author
Chu, Emily

Publication Date
2012

Peer reviewed|Thesis/dissertation

UNIVERSITY OF CALIFORNIA

Los Angeles

External Mass Injection to Reduce Energetic Ion

Production in the Discharge Plume of High Current Hollow Cathodes

A thesis submitted in partial satisfaction

of the requirements for the degree Master of Science

in Mechanical Engineering

by

Emily Chu

2012

ABSTRACT OF THE THESIS

External Mass Injection to Reduce Energetic Ion

Production in the Discharge Plume of High Current Hollow Cathodes

by

Emily Chu

Master of Science in Mechanical Engineering

University of California, Los Angeles, 2012

Professor Richard Wirz, Chair

Hollow cathode discharge studies have shown the existence of energetic ions at high discharge currents that are likely responsible for the high erosion rates and erosion patterns observed on the keeper electrode of the hollow cathode. This thesis uses experimental methods to study the effects of neutral gas injection in the xenon hollow cathode discharge plume on the production of energetic ions to determine the injection conditions that yield optimum hollow cathode operation and life. Parameters considered include the flow split between the cathode internal flow and the external gas injectors, the number of external gas injection sites, the locations of these injection sites, and the orifice size of the injectors, all as a function of the discharge current level. Two lanthanum hexaboride hollow cathodes of diameters 1.5 cm and 2 cm are studied for discharge currents of up to 100 A and 250 A, respectively.

Internal measurements of the 1.5-cm-dia. cathode with a Langmuir probe reveal plasma potential and electron temperature profiles that are characteristic of hollow cathodes and relative insensitivity to the discharge and flow conditions. Plasma density measurements inside the cathode show that the density is sufficiently high and in contact with the entire 2.5-cm insert length only at relatively low internal cathode flow rates so that space-charge limitations on the emitted electron current density are not an issue. At high internal cathode flows, the density peak is pushed toward the orifice plate and the plasma contact with the insert is reduced.

A retarding-potential analyzer is used to make ion energy measurements in the discharge plume of the 2-cm-dia. cathode at discharge currents of 25 to 250 A and at various gas-flow conditions. In general, increasing discharge current increases the energetic ion production at any given flow rate or injection location. External gas injection reduces energetic ion production with fewer energetic ions at higher external injected flow. Further, collimated gas-jet injection performs better than point-source (distributed) injection. Increasing cathode internal flow for constant external flow also reduces energetic ion production. The greatest reduction of energetic ion production occurs when both the internal and external flows were at their maximum values.

Lifetime estimates of the keeper electrode surface due to sputter-erosion by ion bombardment are calculated to determine the impact of the energetic ion generation on the cathode life. High discharge current operation at low cathode gas flow produced very energetic ions that limited keeper lifetimes to less than 5,000 hours. Applying sufficient internal cathode gas flow and external gas injection extended the keeper life to over 10,000 hours at discharge currents of up to 200 A. For higher discharge current operation, more cathode flow and/or injected flow will be required to increase keeper life, but this could not be explored in detail due to pumping speed limitations of the current facility.

This thesis of Emily Chu is approved.

Jeff Eldredge

Ann Karagozian

Xiaolin Zhong

Richard Wirz, Committee Chair

University of California, Los Angeles

2012

Table of Contents

List of Figures

List of Tables

Nomenclature

J emission current density

D_o temperature-modified coefficient to the Richardson-Dushman

T temperature

e electron charge

ϕ_{wf} material work function

k Boltzmann's constant

$f(V)$ ion energy distribution function

$I(V)$ ion current

A_c probe collection area

q_i ion charge state

n_i ion density

V voltage, ion energy

E kinetic energy

T_e electron temperature

V_p plasma potential

$I_{i,sat}$ ion density

β Bohm coefficient

n_e electron density

R rate at which atoms are removed from the surface from bombardment

$Y(V)$ energy dependent sputtering yield of the surface

A_p area

V_o discriminator voltage at which the collected ion current goes to zero

Acknowledgements

First and foremost, I would like to express my deepest and sincerest appreciation for my JPL advisor Dr. Dan Goebel for his support, patience, and guidance through this academic journey. This work would not have been made possible without his expertise and support, and I cannot express my gratitude enough. Thank you to my UCLA advisor Professor Richard Wirz for opening his doors to me whenever I had questions and the members of the electric propulsion group at JPL for their wisdom and encouragement. Thank you to my committee members, Professors Jeff Eldredge, Ann Karagozian, and Xiaolin Zhong, for their time and consideration in reviewing this thesis; any mistakes that remain are my own. And last but certainly not least, I would like to thank my family and friends for their continual support and encouragement through this process.

Thank you all so very much!

E.C.

May 22, 2012

1 Introduction

Electric propulsion (EP) devices, such as ion and Hall thrusters, utilize electricity to increase the propellant exhaust velocity and to generate thrust. With the recent success of EP in attitude control systems (ACS) and as the primary method of in-space propulsion [1], [2], [3], new concepts for EP missions [4] have emerged. Ion and Hall thrusters have been proposed to support large cargo transport for manned missions [5], [6] and to reduce launch vehicle size because of the reduced propellant needs when compared to traditional chemical propulsion. The transport of large masses via ion and Hall thrusters will require these systems to operate at high-power. High-power thrusters consequently will require the use of high current hollow cathodes in the 100 to 500 A operating range.

However, plasma studies in the plume of hollow cathodes have confirmed the existence of energetic ions at high discharge currents that are believed to be responsible for erosion issues [7] observed in hollow cathodes and ion thrusters and which can significantly reduce the lifetimes of these systems. Studies at the Jet Propulsion Laboratory (JPL) have reported a significant reduction in energetic ion production in the hollow cathode discharge plume when cold, neutral gas is injected into the plume region [8], a reduction which will hopefully increase cathode life. This work studies the effects of neutral gas injection in or near the cathode plume on the production of energetic ions in very high current hollow cathodes, and investigates the overall cathode operation and life at various discharge currents and gas flow conditions.

2 Study Objective

This study investigates various techniques to inject cold, neutral gas into the plume region of hollow cathode discharges to reduce the production of high energy ions. Variables of interest include the flow split between the cathode flow and the external injectors, the number of external gas injection sites, the locations of these injection sites, and the orifice size of the injectors. All of these configurations and parameters are recorded and the energetic ion production monitored while discharge current is varied. Experimental methods are used to determine the injection conditions that will yield optimum hollow cathode operation and increased system life.

3 Hollow Cathodes Background

3.1 Hollow Cathode Basics

Cathodes provide electrons in ion and Hall thrusters to ionize propellant gas, create plasma in the thruster, and neutralize the ion beam leaving the thruster. Early ion thrusters utilized a tungsten filament cathode to produce electrons for the plasma discharge and smaller tungsten filament cathodes to provide neutralizing electrons for the ion beam [9]. The high work function of tungsten filaments required operating temperatures of over 2600 K to emit sufficient electrons. High operating temperatures consequentially required high heater power, reducing thruster efficiency, while also driving the filaments to operate at rapid evaporation conditions. Additionally, the exposed tungsten surfaces in the discharge plasma and ion beams were subject to sputtering by ion bombardment. These issues limited filament cathode life to only hundreds of hours or less, which made them inadequate for long-life operation. The development of the hollow cathode reduced these issues by utilizing low work function emitters, corresponding to low emissive temperatures, which were housed inside a hollow structure to protect the active emitting surface against ion bombardment.

A generic hollow cathode consists of a cathode body made of a hollow refractory tube, an insert that is the active electron emitter, a heater to heat the insert to emissive temperatures, and a keeper electrode to help light the cathode during start-up and to protect the cathode from ion bombardment from the cathode plume plasma. An assembly drawing of the 1.5-cm-dia. LaB_6 cathode used in this study is provided in Figure 1.
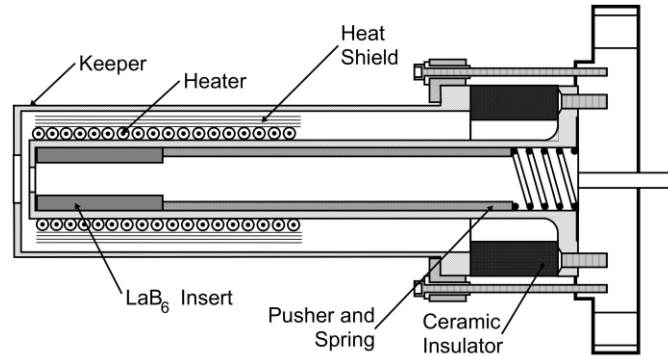
Figure 1: Assembly drawing of the 1.5-cm-diameter LaB$_6$ hollow cathode.

The cathode body is fitted with an orifice plate on its downstream end and houses the cylindrical electron emitter. The emitter is made of a low work function material and is pressed up against the orifice plate by a spring and is made of a low work function material. The heater is wrapped around the cathode body and used to bring the insert to emissive temperatures during start up. Heat shields are wrapped around the heaters to direct heat to the insert and reduce radiation losses. The keeper, which is electrically isolated from the cathode by a ceramic spacer, is fitted over the cathode body and bolted to the base flange, which has a gas feed line welded to it to allow propellant to enter the cathode body during operation.

To run the cathode, the heater is first turned on to bring the active insert to emissive temperatures. A voltage difference is then introduced between the keeper and the cathode body (which is normally grounded), and neutral gas is injected into the cathode through the gas feed line. Once the keeper is able to collect one to four Amperes of electron current, the cathode discharge power supply is turned on to low current ($\approx$25 A), allowed to stabilize for a few minutes, and then turned up to full power. The heater is then turned off because the insert is self-heated by the plasma discharge and therefore self-sustains when the discharge is running. Note that electrons emitted off of the insert ionize the injected gas to form a cathode plasma. The

4

electrons that form the discharge current are extracted from the cathode plasma through the orifice and into the thruster plasma.

3.2   Thermionic Emitters and Lanthanum Hexaboride

Hollow cathodes developed in the U.S. for space application traditionally use a porous tungsten insert, impregnated with an emissive mix of barium, calcium oxides, and alumina [3], [1], as their thermionic emitters. This barium oxide impregnated (BaO-W) dispenser cathode "dispenses" barium from the tungsten matrix to activate the emitter surface. At temperatures over 1000 ^{o}C, chemical reactions at the surface reduce the work function to about 2.08 eV. However, because the formation of the low work function surface involves chemistry, BaO-W dispenser cathodes are highly sensitive to poisoning by water vapor and impurities in the gas that reduce the work function of the emitter, shorten cathode lifetime, or prevent cathode emission [10]. Additionally, operating BaO-W dispenser cathodes at discharge current above 50 to 100 A usually results in overheating of the insert and reduced life, making this type of emitter undesirable for the high-current applications required by high-power NASA missions.

An alternative electron emission material is lanthanum hexaboride (LaB$_6$). This type of emitter has extensive use in space and on the ground; it has been flown in over a hundred Russian Hall thrusters over the last 35 years [11], [12] and has been used widely in university research devices and industrial applications. Several high current LaB$_6$ hollow cathodes have been developed at JPL for high power Hall thrusters [13], [14], [15].

Lanthanum hexaboride is made by press-sintering LaB$_6$ powder into plates and rods [16]. The resulting polycrystalline material is usually electron-discharge machined to the desired shape, has a work function of about 2.67 eV, and will emit over 10 A/cm^2 at temperatures of

1650 °C. Compared to conventional impregnated dispenser cathodes, LaB$_6$ cathodes are incredibly robust, have high current density, and exhibit long life.

The thermionic emission characteristic of a material can be described by the modified Richardson-Dushman equation [17]:

$$J = D_o T^2 e^{-\frac{e\phi_{wf}}{kT}} \tag{1}$$

where D_o is the temperature-modified coefficient to the Richardson-Dushman equation [18], T is temperature,   is the electron charge, ϕ_{wf} is the work function, and k is Boltzmann's constant.

Table 1 tabulates values of D_o and the work function of several electron emitter materials found in the literature. Differences in work function values for LaB$_6$ are due to varying use of D_o because of variations in the surface stoichiometry [19], density differences of polycrystalline LaB$_6$ emitters, or crystal orientations in single-crystal emitters used for some applications [20].

Figure 2 plots the emission current density, calculated from Equation (1, as a function of emitter temperature for the materials listed in Table 1. The LaB$_6$ emission current densities predicted by the different authors in Table 1 are within 25% of each other.

Table 1: Work function and Richardson coefficients for different cathode materials.

	D_o	ϕ_{wf}
BaO-W 411 [10]	120	$1.67 + 2.82 \times 10^{-4}$ T
BaO-W 411 [13]	1.5	1.56
LaB$_6$ [16]	29	2.67
LaB$_6$ [19]	110	2.87
LaB$_6$ [39]	120	2.91
LaB$_6$ [21]	120	$2.66 + 1.23 \times 10^{-4}$ T
Molybdenum [21]	55	4.2
Tantalum [21]	37	4.1
Tungsten [21]	70	4.55
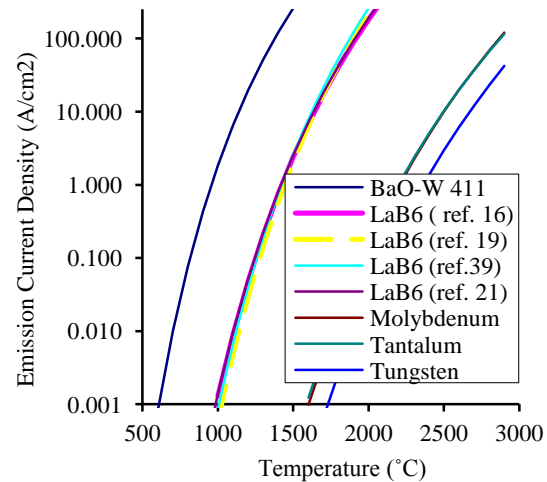
Figure 2: Emission current density versus temperature.

For the same emission current density, LaB_6 operates at several hundred degrees lower temperature than typical refractory metal emitters that are used as filaments in some plasma discharges, and evaporates at a significantly lower rate than refractory metals at thermionic emission temperatures [21], [22]. Although BaO-W dispenser cathodes operate at much lower temperatures than LaB_6 cathodes, LaB_6 inserts have lower evaporation rates than the impregnate materials in dispenser cathodes until the emission current density exceeds 15 A/cm^2 [23]. Because cathode lifetime is primarily determined by the evaporation rate of the insert, LaB_6 cathode life is typically better than BaO-W cathode life because there is more material in the bulk LaB_6 than in the impregnated dispenser cathode and the evaporation rate of LaB_6 is also lower than or comparable to that of BaO-W inserts for emission current densities of up to 20 A/cm^2.

Lanthanum hexaboride must be interfaced with materials that inhibit diffusion of the boron compounds into the support material [23]. This diffusion embrittles most contacting refractory metals that can be used at the higher operating temperatures of LaB_6, leading to structural failure. Crystalline LaB_6 is also susceptible to breakage from thermal shock and mechanical stress when clamped. To avoid these issues, LaB_6 has been supported by carbon [24], [25], tantalum carbide [16], [22], and rhenium [26]. Fine-grain graphite provides good electrical contact, has comparable thermal expansion [14] characteristics as LaB_6, and provides low stress support [15], [25] without significant boron diffusion or boride formation. Poco graphite is used to make contact with the LaB_6 insert in this study for these reasons.

The entire LaB_6 volume is capable of providing an active emitting surface, and thus LaB_6 cathodes are insensitive to air exposures and impurities that would normally destroy BaO-W dispenser cathodes (which require chemistry to create the low work function surface).

Additionally, the LaB_6 material does not require significant conditioning, activation, or purging that is normally required of dispenser cathodes. This robustness makes the processing and handling of EP devices that use LaB_6 cathodes significantly easier than for those that use dispenser cathodes. However, the need to interface LaB_6 with compatible materials and the higher operating temperature of LaB_6 has limited its use in the U.S. space program.

To support the high discharge current and long life needs of next generation high power Hall thrusters, LaB_6 hollow cathodes developed at JPL have been tested to discharge currents of up to 250 A, and external and internal measurements of plasma properties of the cathode were recorded. Results from two LaB_6 hollow cathodes are presented in this thesis. A 1.5-cm-dia. LaB_6 hollow cathode is characterized for discharge currents of up to 100 A and a 2-cm-dia. LaB_6 hollow cathode is characterized for discharge currents of up to 250 A. Life estimates for these cathodes and issues associated with high-current operation are presented and discussed.

3.3   High Power Application and Energetic Ions

Motivation

High current hollow cathodes are necessary for the next generation, high-power ion and Hall thrusters that have been proposed for use in future EP missions [4]. For instance, a 20 kW Hall thruster requires a hollow cathode with nominal operating currents of 50 to 100 A, a 50 kW Hall thruster needs a 125 to 250 A hollow cathode, and a 100 kW Hall thruster requires a 250 to 500A hollow cathode [23].

High Energy Ions

Hollow cathode discharge studies by various groups have demonstrated the existence of high energy ions that may be responsible for erosion patterns observed on the keeper electrode face-plate and orifice. Kameyama and Wilbur of Colorado State University used an electrostatic

8

energy analyzer to conduct ion energy distribution measurements in the plume of a xenon hollow cathode at discharge currents up to 30 A. They found ions with energies greater than any voltage difference applied to the electrodes [27], which is consistent with other studies of the like [7], [28]. They also observed that energetic ion production in the plume increased with increasing discharge current, a characteristic of great concern for hollow cathodes being developed for high power use because the energetic ions produced at high current will bombard the keeper electrode and cause erosions which ultimately lead to cathode failure.

Figure 3 provides a series of photographs that capture the erosion progression from ion bombardment experienced by the NASA Solar Electric Propulsion Technology Application Readiness (NSTAR) hollow cathode at various stages during an extended life test (ELT) [7]. At 15,617 hours, the keeper electrode has eroded to the point where the cathode orifice plate and heater is completely exposed.

| 0 hours | 4693 hrs | 6408 hrs | 11673 hrs | 15617 hrs |
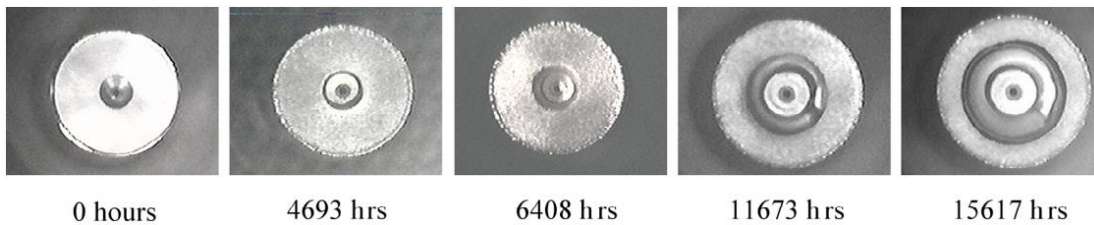
Figure 3: Evolution of the NSTAR hollow cathode during the extended life test. The keeper electrode orifice has enlarged to beyond the cathode diameter in 15,617 hours.

Several explanations for high energy ion production in the plume have been proposed, including ion instabilities in a double layer postulated in the orifice of the hollow cathode [29] or a DC potential hill [30] located just downstream or inside of the cathode orifice. These effects have not been substantiated, but large plasma potential oscillations in the hollow cathode plume were found to be correlated with energetic ion production in the cathode exit [28]. At JPL, Goebel demonstrated that these oscillations could be quenched and the energetic ion production

reduced drastically by injecting cold neutral gas directly into the cathode plume by an exterior gas feed line [8]. As mentioned previously, this thesis examines the effects of neutral gas injection in the cathode plume on the production of energetic ions from very high current hollow cathodes, and on the overall cathode discharge operation, while considering the flow splits between the internal cathode flow and the external injection flow rates, the number of external injection sites, and the locations of these external injectors.

4   Experimental Configurations

4.1   Cathode Specifications

Two LaB$_6$ hollow cathodes are studied in this thesis: a 1.5-cm-dia. cathode for currents up to 100 A and a 2-cm-dia. cathode for currents up to 250 A. Assembly drawings of the two cathodes are provided in Figure 4. The cathodes run off of xenon gas, which is typical of hollow cathodes used in EP devices.
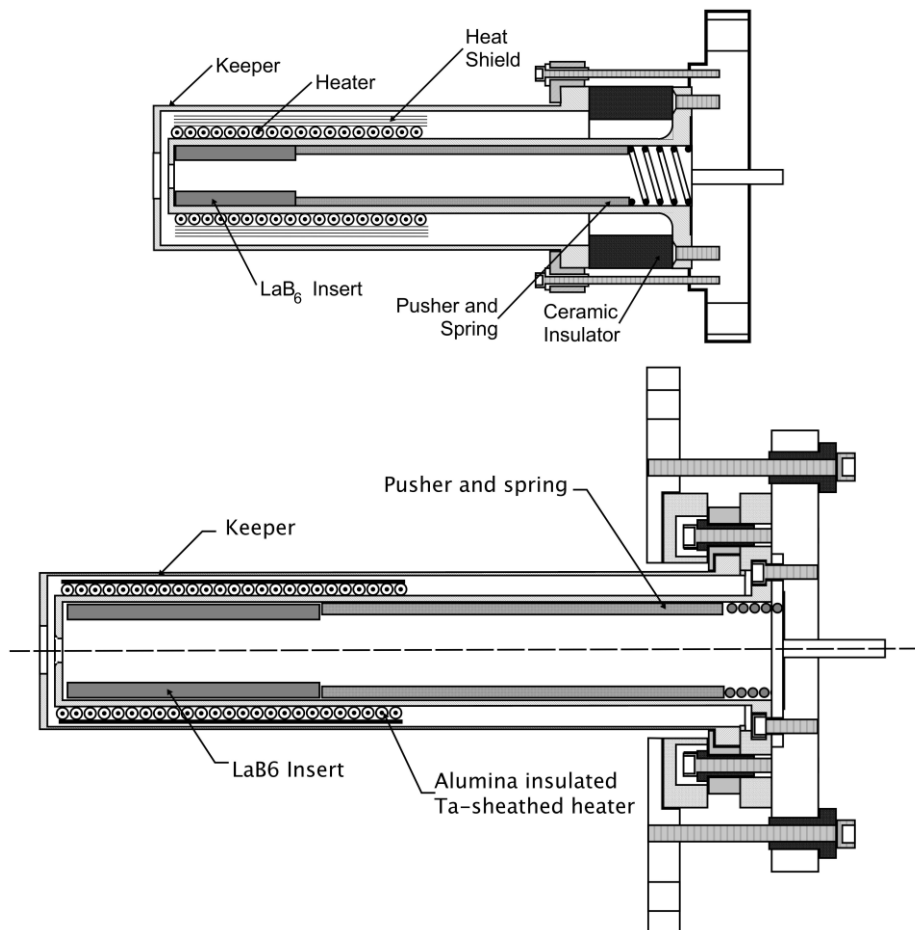

Figure 4: Assembly drawings of the 1.5-cm-dia. and 2-cm-dia. LaB6 hollow cathodes, respectively.

These larger diameter hollow cathodes are constructed using the basic design presented in Section 3.1 and described in detail by Goebel [13], [14]. Both cathode bodies are made of Poco

11

graphite to eliminate interface issues with the LaB_6 insert. Additionally, the graphite cathode has comparable thermal expansion characteristics as the LaB_6 material and so is suitable for the insert on a structural level. Each cathode is fitted with a tungsten orifice plate against a step in the graphite tube and isolated from the LaB_6 insert by a thin graphoil washer. This arrangement is held in place by a spring as shown in the assembly drawings. The cathodes are wrapped with high-temperature alumina-insulated, tantalum-sheathed (Al_2O_3-insulated, Ta-sheathed) heaters. The insulation material in the heaters has a maximum operation temperature of 1800 ˚C, above which chemical reactions between the insulator and the heater electrode reduce the resistance, ultimately leading to heater failure [31]. Heater characterization at JPL has shown that the Al_2O_3-insulated, Ta-sheathed heaters have great life if they are operated at 11 A or less. The long and thin-wall design of the cathode tubes minimizes conduction heat loss from the insert to the base plate. The keeper electrodes are also made from Poco graphite. The cathode body and keeper electrode are bolted together through insulated flanges that are attached to the power supply electrical leads and the gas feed system.

1.5-cm-dia. Cathode

The 1.5-cm-dia. cathode was designed to operate at a nominal discharge current of 100 A. The cathode tube has an outer diameter (O.D.) of 1.5 cm, a wall thickness of 0.1 cm, and a length of 10.7 cm. The LaB_6 insert is 2.5 cm long, 1.27 cm in diameter, and has a 0.32 wall thickness, which yields an active emitting area of 5 cm^2 inside the cathode. According to

Figure 2, this can produce emission currents of 100 A at temperatures of 1700 ˚C. This cathode requires 240 W of heater power to reach emissive temperatures.

Figure 5 provides two photographs of the 1.5-cm-dia. LaB$_6$ cathode. On the left, the cathode body is shown mounted on a test fixture and wrapped with the heater and heat shield; on the right, the cathode fully assembled with keeper attached.
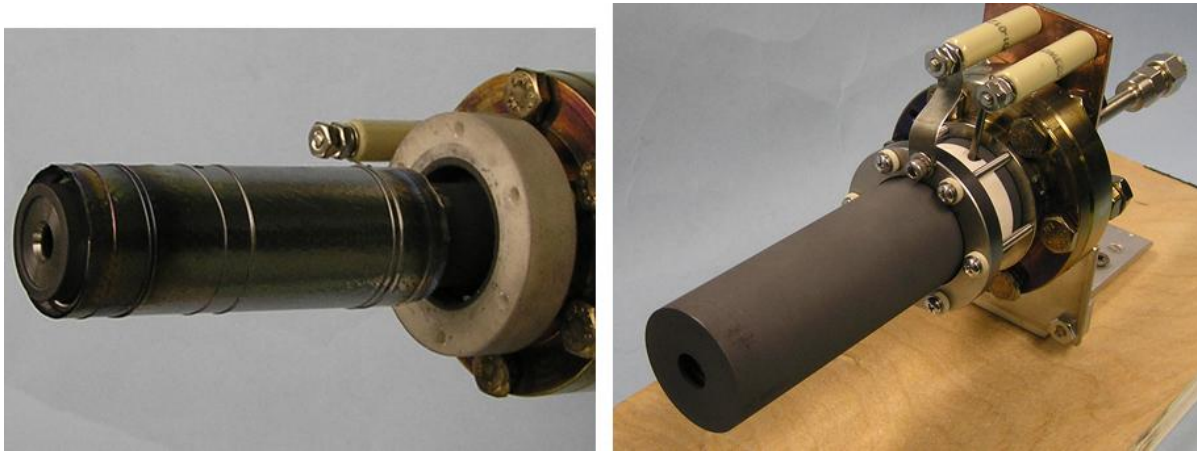
Figure 5: The 1.5-cm-dia. LaB6 hollow cathode wrapped with heater and heat shield and without the keeper (left) and fully assembled (right).

2-cm-dia. Cathode

One focus of this thesis was aimed at mitigating energetic ion production in the plume of the 2-cm-dia. LaB$_6$ hollow cathode at discharge currents of 25 to 250 A. This cathode is constructed using the same basic design described in the previous section but features more insert surface area to provide higher discharge currents and longer life. The cathode tube has an outside diameter of 2 cm and the same wall-thickness and length as the 1.5-cm-dia. cathode. The cathode tube houses two LaB$_6$ inserts (O.D. 1.9 cm and I.D. 1 cm) of lengths 2.6 cm and 2.9 cm. Two Al$_2$O$_3$-insulated, Ta-sheathed heaters are connected in parallel around the cathode tube to provide the 400 W of heater power needed to light the cathode. The graphite keeper is 3.5 cm in O.D. to accommodate the heater, heat shields, and larger diameter cathode insert and tube.

Photographs of the 2-cm-dia. cathode are provided in Figure 6. On the left are some parts for the 2-cm-dia. cathode, including a Tungsten orifice plate, a couple LaB$_6$ inserts, a graphite spring, a cathode tube, and heat shielding wrapped around the Al$_2$O$_3$-insulated, Ta-sheathed heater. The photograph on the right shows the 2-cm-dia. cathode fully assembled.
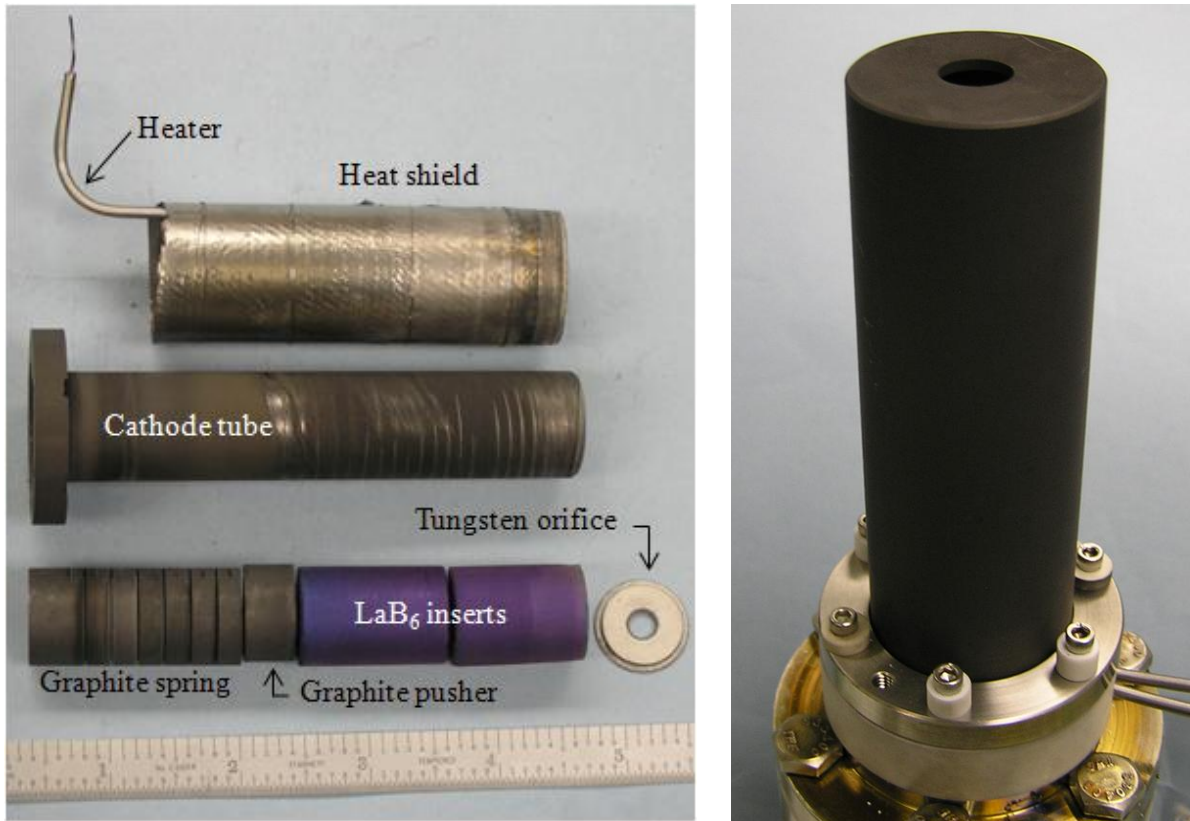
Figure 6: Parts for the 2-cm-dia. LaB6 hollow cathode (left); the same cathode fully assembled (right).

4.2   Vacuum Facility and Hardware

Experiments are conducted in two vacuum systems, the JPL cathode test facility [32] for discharge currents up to 100 A and the JPL high current test facility for discharge currents up to 250 A. Photographs of these systems are provided in Figure 7. Data from the diagnostics in this study are collected on a personal computer via a National Instruments data acquisition system.

14
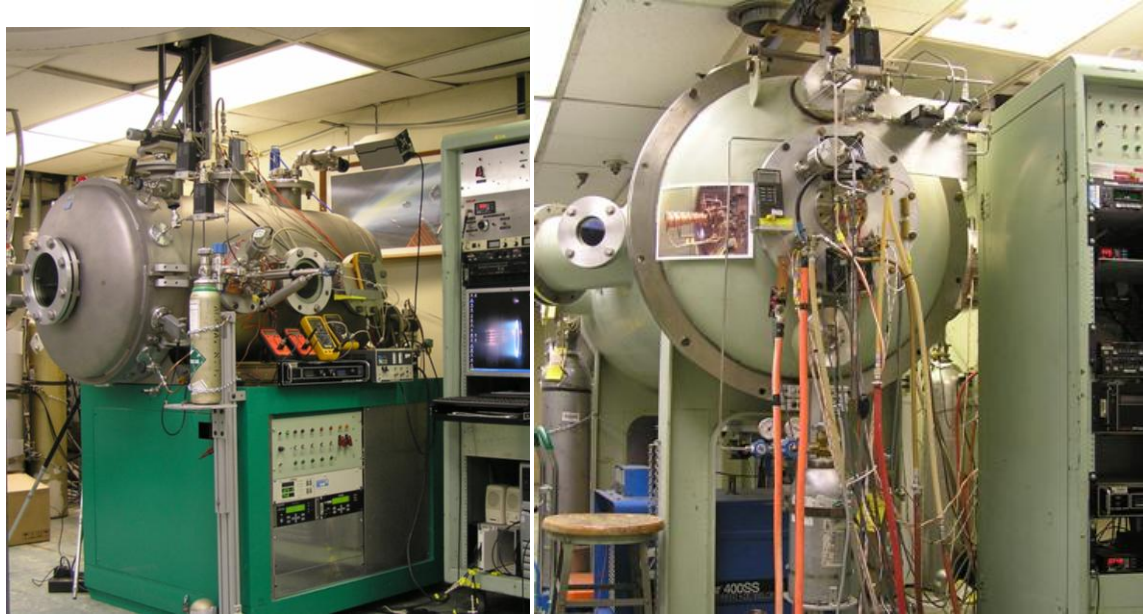
Figure 7: JPL cathode test facility (left) and JPL high current test facility (right).

JPL Cathode Test Facility

Both cathodes were operated in the JPL cathode test facility for discharge currents up to the maximum limit (100 A) of the discharge power supply. The 1-m-dia. by 2.5-m-long vacuum chamber is pumped by two 10-inch CTI cryopumps that have a combined pumping speed of 1275 l/s for xenon. Chamber base pressure is in the 10^{-8} Torr range. During normal operation of the cathodes, the chamber pressure remains in the 10^{-4} Torr range. The xenon gas flow is measured in units of standard cubic centimeters per minute (sccm) and controlled by a calibrated digital mass flow controller, while a precision Baratron capacitive manometer monitors the pressure inside the hollow cathode. A 5-cm-diameter solenoid coil is positioned around the keeper and provides an adjustable axial magnetic field at the cathode exit to simulate the field found at the cathode in ion and Hall thrusters. The 6.5-cm-diameter anode cylinder is water-cooled to prevent the system from overheating during high current cathode operation. Depending on the cathode current and flow rate, this experimental configuration produces

15

discharge voltages of 15 to 40 V. The retarding potential analyzer (RPA), for ion energy distribution measurements, is positioned in the gap between the keeper orifice and upstream end of the anode and is oriented so that its collection orifice is perpendicular to the cathode radius. A flat probe is placed a few centimeters away from the cathode axis, and is positioned in various locations to measure the plasma flux the anode or the RPA. Figure 8 provides a photograph of this setup. This arrangement in the cathode test facility permitted performance characterization of external plasma properties of the two cathodes at up to 100 A of discharge current.
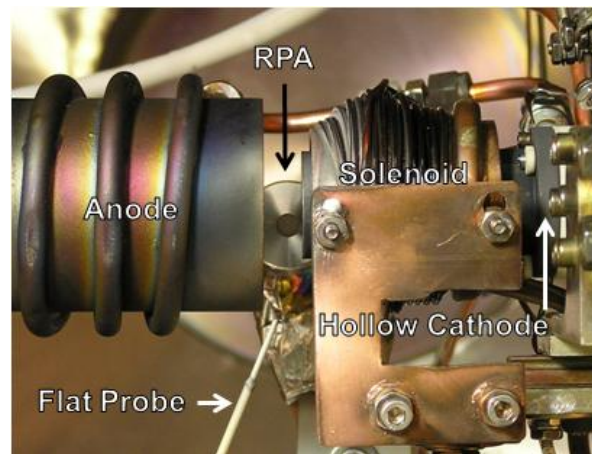
Figure 8: Experimental set-up inside the JPL cathode test facility.

Additionally, an interior fast scanning probe was used to measure the electron temperature, plasma potential, and ion density inside the 1.5-cm-dia. cathode for discharge currents of up to 100 A. Figure 9 provides a schematic drawing of the experimental setup for internal probing.
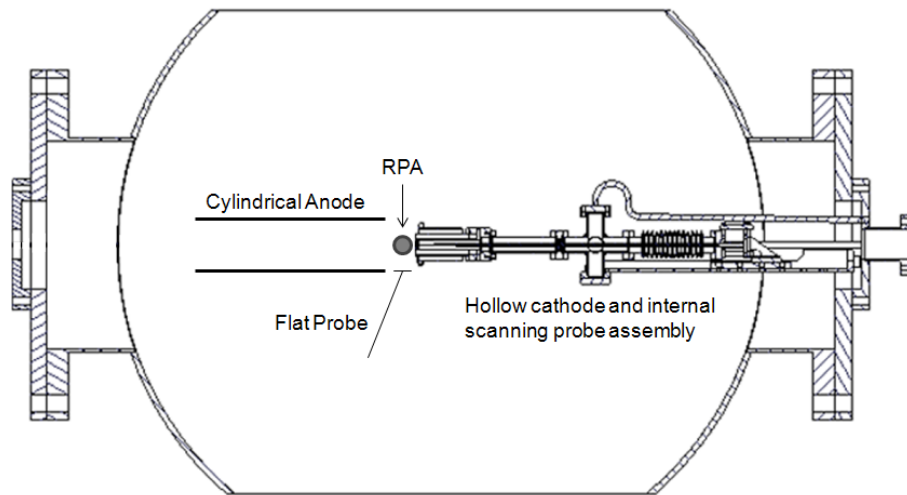
Figure 9: Experimental setup schematic for internal probing.

The base flange of the 1.5-cm-dia. cathode was fitted to the scanning probe assembly. Details of the mechanics of this probing technique are presented in detail in several of Goebel's papers [7], [28]. Basically, the cathode probe is aligned axially by two slide-guides, has a linear throw of 3 cm, and can traverse the interior of the cathode at speeds of 1-2 m/s. This produces a 0.25 mm position resolution and a 10 ms residence time in the orifice region. Figure 10 provides a photograph of the Langmuir probe fully inserted inside the 1.5-cm-dia. hollow cathode.
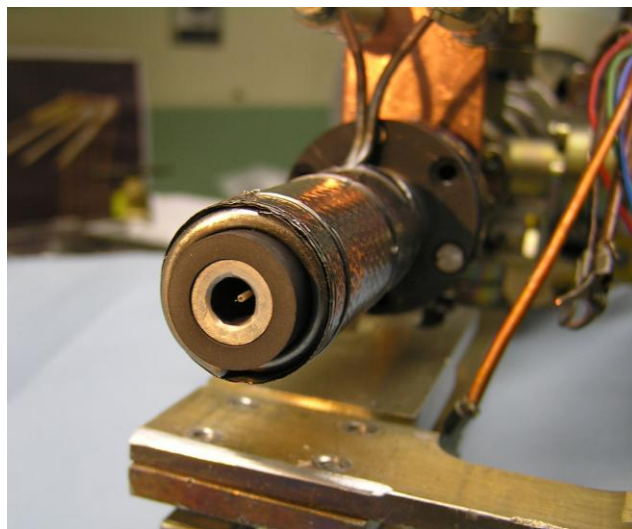
Figure 10: Langmuir probe extending inside the 1.5-cm LaB6 cathode.

17

JPL High Current Test Facility

The 2-cm-dia. cathode was then run and characterized in the JPL high current test facility for discharge currents of up to 250 A. This chamber is 2.8 m long and has a diameter of 1.3 m. Its pumping speed capability for xenon is comparable to that of the JPL cathode test facility. Chamber base pressure is in the low 10^{-7} Torr range, and remains in the 10^{-5} to 10^{-4} Torr range during normal cathode operation. A photograph of the experimental setup inside of the larger-diameter vacuum chamber is provided in Figure 11.
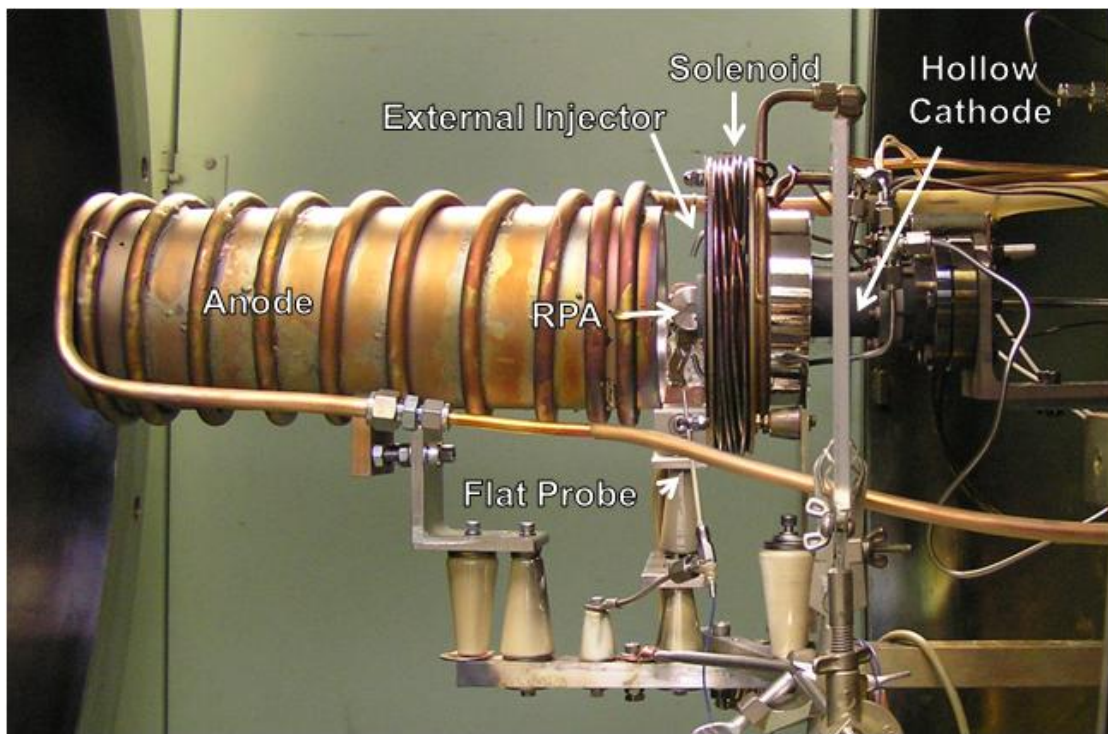
Figure 11: Experimental set-up inside the JPL high current test facility

A solenoid that produces an adjustable magnetic field is positioned around the keeper electrode and the system features a 10-cm-diameter water-cooled, cylindrical anode. Again, similar to the setup in the other vacuum chamber, the RPA is positioned in the gap between the keeper orifice and upstream end of the anode. A flat probe to measure plasma flux is placed at the same radial distance from the cathode axis as the RPA to determine flux into the RPA and

18

also flush against the keeper orifice plate to measure fluxes to this electrode used to determine sputter rates of the orifice plate. Depending on the discharge current and the flow splits between the cathode and external injectors, this arrangement produces discharge voltages in the 15 to 30 V range.

5 Diagnostics

5.1 Retarding Potential Analyzer

To determine the ion energy distribution in the plume of the hollow cathode discharge, a retarding potential analyzer (RPA) was placed radially about 10 cm from the cathode plume plasma in the gap between the keeper and anode as shown in Figure 8 and Figure 11. The RPA in this study features four grids and a current collector plate. It determines the ion energy distribution by filtering ions according to their kinetic energy. An electrical schematic of the four-grid RPA is provided in Figure 12. The first grid is in contact with the plasma and is floated to minimize perturbations to the plasma, the second grid is biased to repel elections, and the third and fourth grids are connected together to form the equi-potential discriminator grid, which is swept positively so that only ions with voltage ratios greater than the potential applied to the grid can reach the collector plate. The collector current data versus the discriminator voltage obtained from the RPA trace is processed to give the ion energy distribution.
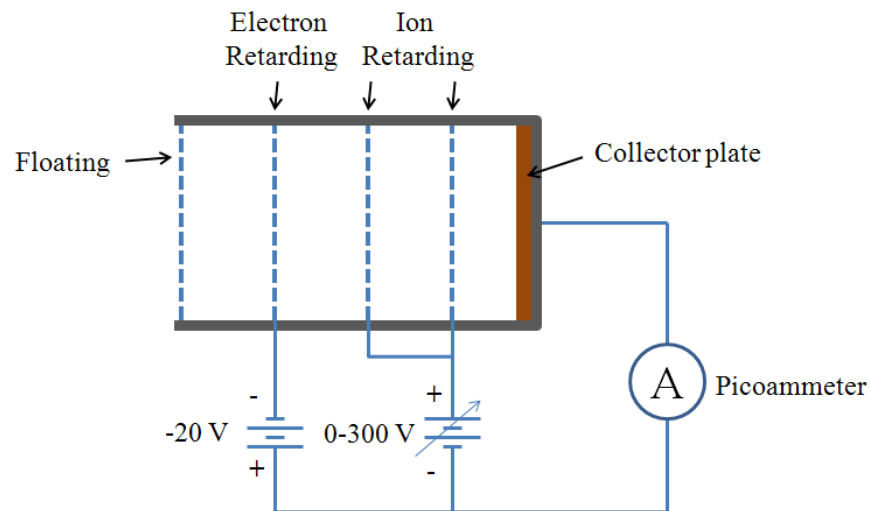
Figure 12: Electrical schematic for the four-grid RPA.

As presented in King's PhD thesis [33] and explained in detail in most plasma diagnostic textbooks [34], the ion energy distribution function, $f(V)$, for single ion species is related to the RPA collected current. Consider an RPA trace of a sample plasma condition. The ion current incident on the collector plate, after the electrons have been repelled and the ions have been selectively filtered by the discriminator grid, is defined to be

$$I(V) = A_c q_i e n_i \int_{u_{min}(V)}^{\infty} u_i f(u_i) du_i \tag{2}$$

where A_c is the probe collection area, q_i is the ion charge state, e is the electron charge, and n_i is the ion density. Using the following transformation variables $u_i = \sqrt{\frac{2q_i eV}{m_i}} \Rightarrow du_i = \frac{1}{2}\sqrt{\frac{2q_i e}{m_i}}V^{-\frac{1}{2}}dV$ where V is the discriminator voltage, Equation 2 can be simplified to

$$I(V) = A_c q_i e n_i \int_{V}^{\infty} \sqrt{\frac{2q_i eV}{m_i}}\frac{1}{2}\sqrt{\frac{2q_i e}{m_i}}V^{-\frac{1}{2}}f(V')dV' \tag{3}$$

$$I(V) = \frac{q_i^2 e^2 n_i A_c}{m_i}\int_{V}^{\infty}f(V')dV' \tag{4}$$

Then, differentiating Equation 4 with respect to the discriminator voltage yields a relationship between the collector current I and the ion voltage distribution function $f(V)$:

$$-\frac{dI}{dV} = \frac{q_i^2 e^2 n_i A_c}{m_i}f(V) \tag{5}$$

Here, $I\text{-}V$ data is obtained by varying the ion retarding grid potential and recording the corresponding collector plate current. Equation 5 reveals that for constant q_i and m_i (i.e. single species flow), the ion voltage distribution function $f(V)$ is directly proportional to the negative voltage rate of change of the collector current dI/dV. Additionally, voltage is defined as $V = E/q$,

21

where E is the particle kinetic energy. For our case of the single species flow where q_i is constant, $f(V) = f(E_i/q_i)$, which is exactly the ion energy distribution function.

Note that interpretation of the RPA data as an ion energy distribution is valid only for the case of same-species ions. Also, because of noisy probe signal likely from turbulent ion acoustic waves in the cathode plume, collected current-voltage data is fit to a polynomial before being used to determine the ion energy distribution.

5.2 Langmuir Probe

A Langmuir probe is a plasma diagnostic used to determine the electron temperature, plasma potential, and ion current density of a plasma sample. It is used extensively in plasma research and its theory of operation can be found in most plasma diagnostic textbooks [35]. The probe is made of a conducting material and is inserted into the plasma sample. During data collection, the probe potential is varied while the current induced on the probe by the surrounding ions and electrons is monitored. Current-voltage data from the Langmuir trace can then be post-processed to yield an electron temperature, a plasma potential, and an ion current density.

A sample Langmuir trace is provided in Figure 13. To make the data easier to work with, the probe current has been inverted and plotted on a semi-logarithmic scale against the probe potential. Regions I, II, and III are the ion saturation, electron retarding, and electron saturation regions, respectively.

22
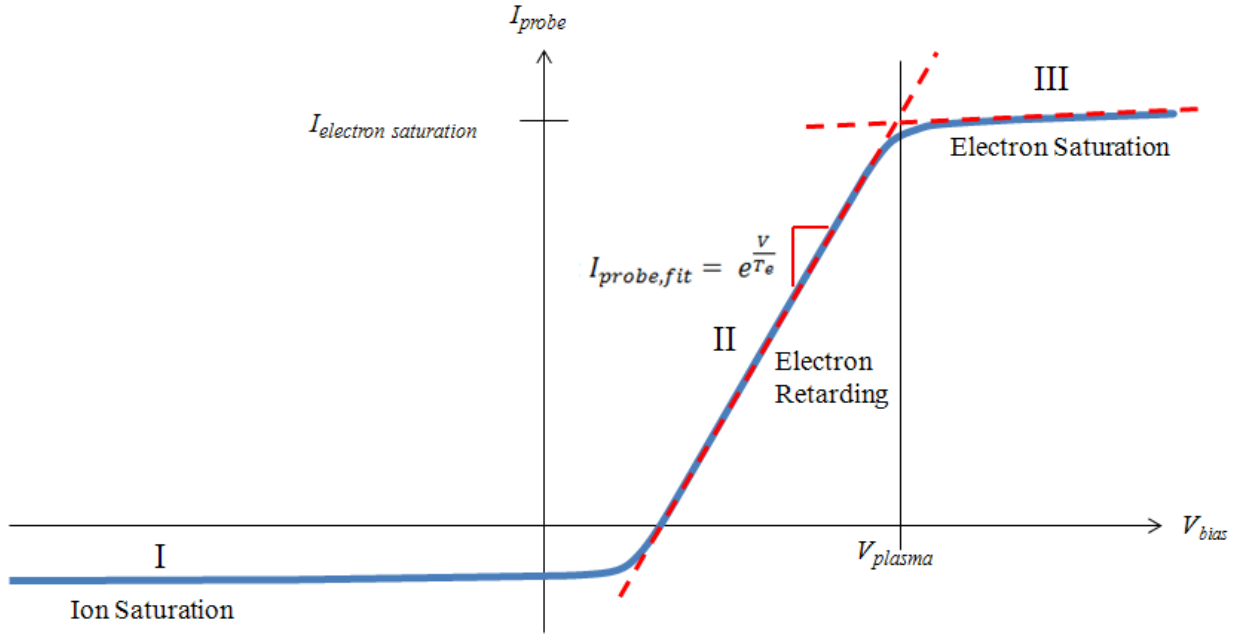
Figure 13: Theoretical Langmuir trace of a plasma sample.

The parameters of a Langmuir trace that are of interest to this study are the electron temperature T_e, plasma potential V_p, and ion density $I_{i,sat}$ of the plasma inside the 1.5-cm-dia. hollow cathode.

To determine the electron temperature of the plasma sample from a Langmuir trace, a semi-logarithmic curve is fit to the electron retarding region of the collected data. This curve fit will take the form: $I_{probe,fit} = e^{\frac{V}{T_e}}$. The electron temperature can then be easily extracted from this curve fit equation.

To determine the plasma potential, a semi-logarithmic curve is fit to the electron saturation region of the trace. The voltage bias at which the curve fit for the electron retarding region and the curve fit for the electron saturation region intersect is the plasma potential. See Figure 13.

As presented in Jameson's thesis [36] and found in Goebel's 2005 Journal of Applied Physics paper [37], the ion saturation, also known as the ion density, is given by

$$I_{i,sat} = \beta n_e e \sqrt{\frac{kT_e}{M}} A \qquad (5)$$

Where β is the Bohm coefficient, n_e is the electron density, and A is the probe area. Again, the theory behind this analysis method is well documented in plasma diagnostic texts and relevant journal articles [36].

6 Experimental Results

Experimental results are reported here for the 1.5-cm-dia. and 2-cm-dia. LaB$_6$ hollow cathodes; data analysis is provided in the following chapter. The cathodes utilized in this study are run on xenon gas and results are reported in two sections: the first is for operation in the JPL cathode test facility at up to 100 A of discharge current and second is for operation in the JPL high current test facility at up to 250 A of discharge current. Both hollow cathodes were operated in the JPL cathode test facility for discharge currents of up to 100 A to allow for current-voltage (I-V) characterization of the cathodes. Additionally, internal plasma measurements of the 1.5-cm-dia. cathode were made in this chamber to determine the optimum cathode flow rates that yield long insert life. The 2-cm-dia. cathode was then operated in the JPL high current test facility where experiments aimed at eliminating energetic ion produce were made, and the results are reported in the latter half of this chapter. It should be noted that the 1.5-cm-dia. cathode has a maximum nominal operation of 100 A, which is why it was not run in the higher current facility. This thesis focuses on the characterization of the 2-cm-dia. hollow cathode because this is the cathode that we inject neutral xenon gas into the discharge plume to study the effects of external gas injection on energetic ion production in the plume.

6.1 Characterization of the 1.5-cm-dia. cathode

This section reports measurements made on the 1.5-cm-dia. hollow cathode, including characteristics of the cathode for three xenon flow rates and internal plasma measurements in the insert region to aid in the understanding of the electron emission processes of the LaB$_6$ inserts of larger-diameter hollow cathodes. Internal plasma density, potential, and electron temperature profiles were measured with the fast-scanning Langmuir probe drive system

described in Section 4.2. While external injection was introduced into the plume region for select cases of the 1.5-cm-dia. cathode operation to verify the effectiveness of gas injection on energetic ion suppression, comprehensive gas-injection experiments were not performed on this cathode and these results are not reported here.

In Figure 14, the discharge and keeper voltages are plotted against discharge current for the 1.5-cm-dia. hollow cathode for discharge currents of 10 to 100 A. When the discharge current drops below 20 A, the discharge voltage increases with decreasing discharge current. At discharge currents below 10 A, both the 1.5-cm-dia. and 2-cm-dia. cathodes stopped operating because of insufficient self-heating in the cathode to maintain the insert temperature.
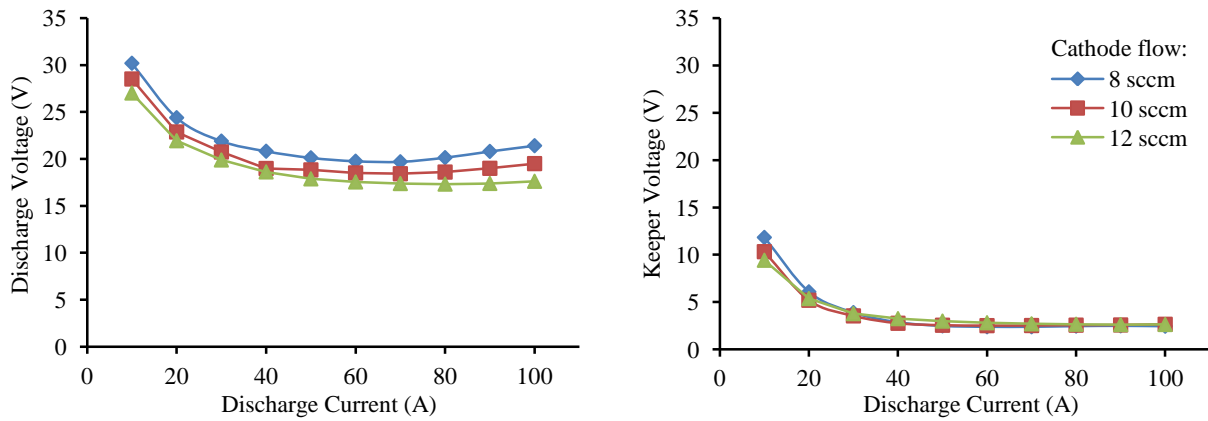
Figure 14: Discharge (left) and keeper (right) voltages at three xenon flow rates for the 1.5-cm-dia. cathode.

Plasma potential and electron temperature profiles obtained inside the 1.5-cm-dia. cathode for three different xenon flow rates are provided in Figure 15 for discharge currents of 50 and 100 A. The zero value on the x-axis is at the cathode orifice. The observed plasma potential profile is characteristic of hollow cathodes insert plasmas [32], with plasma potential increasing with decreasing distance to the orifice. At 50 A of discharge current, the plasma potential is about 1 V higher than that of the 100 A case. Higher plasma potential is required at

lower current to provide sufficient self-heating [9]. As seen in Figure 15, the electron emperature

is similar for both 50 and 100 A operation and increases slightly with decreasing distance to the

orifice.
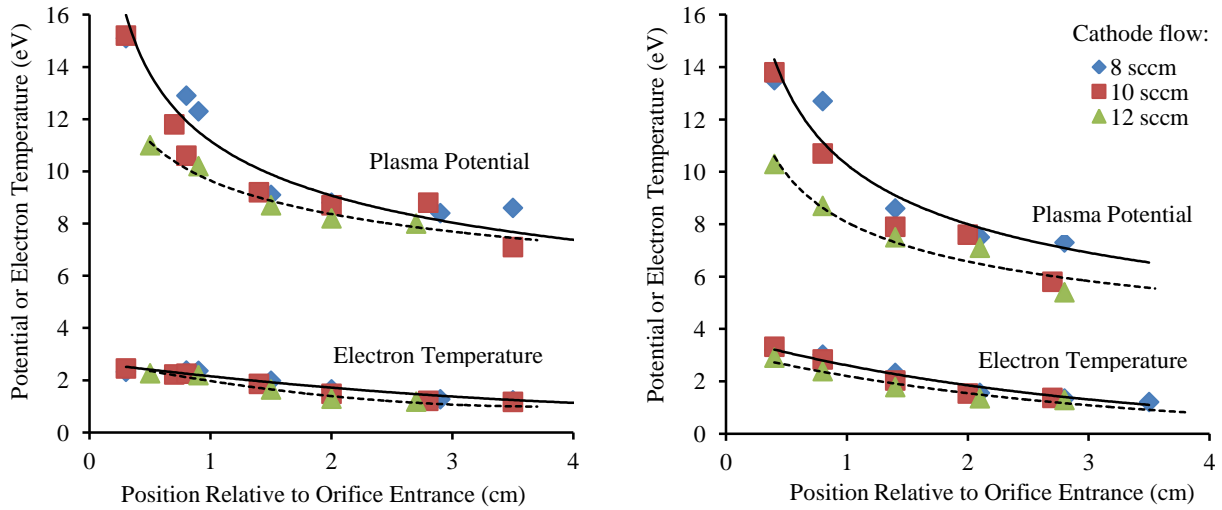
Figure 15: Plasma potential and electron temperature profiles in the 1.5-cm cathode at three xenon flow rates and 50 A (left) and 100 A (right).

A plot of electron temperature against discharge current at an internal location of 1 cm

upstream of the cathode orifice is provided in Figure 16 and shows that the electron temperature

in the insert region decreases slightly with discharge current.
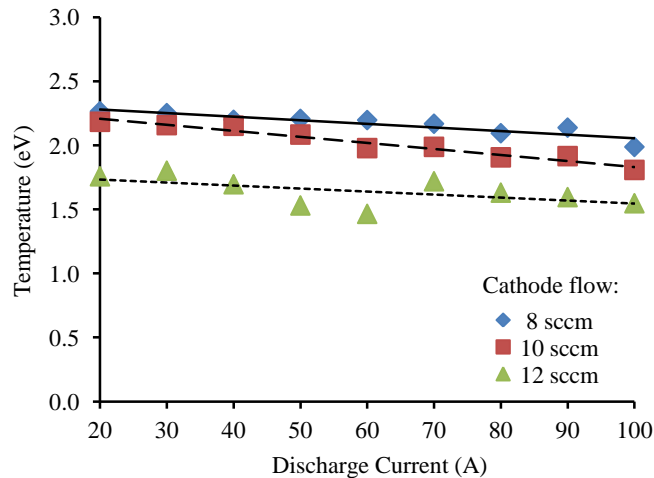
Figure 16: Electron temperature versus discharge current for three xenon flow rates.

Ion saturation measurements made inside the hollow cathode are used [32] to produce plasma density profiles for discharge currents of 20 to 100 A, where the density profiles are calculated from Equation (5 from Section 5.2 using the electron temperatures found in Figure 15. Density profiles at 8 sccm and 12 sccm of xenon flows in Figure 17 show that the plasma density is very high and is in contact with the entire 2.5-cm insert length so space-charge limitations on the emitted electron current density [9] are avoided. Further, increasing gas flow and discharge current brings the plasma density peak towards the orifice, which flattens the density profile further. At high cathode flows, the plasma density peak gets pushed up against the orifice and contact area between the xenon gas and LaB_6 material is reduced so that space-charge limitations on the emitted electron current density become an issue and insert life is reduced.
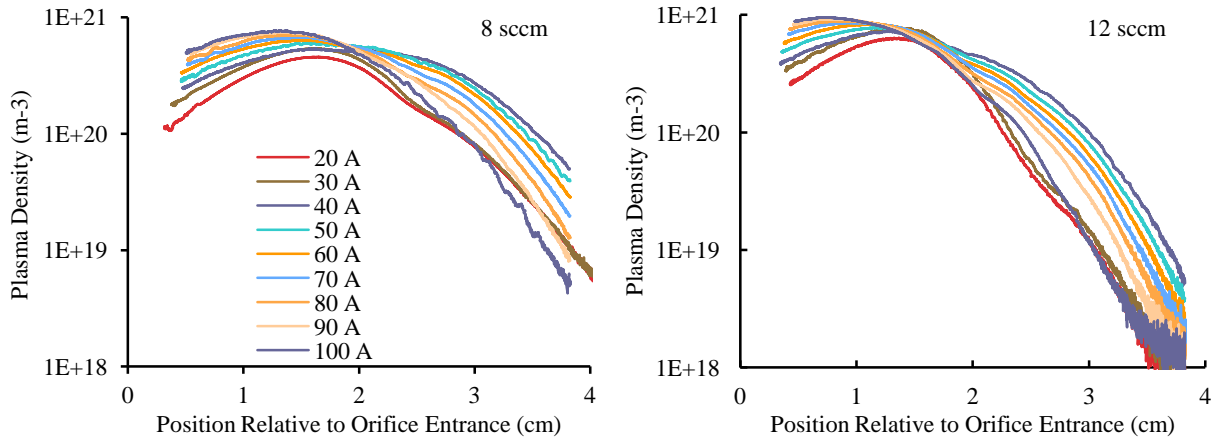
Figure 17: Plasma density profiles inside the 1.5-cm cathode for 8 sccm (left) and 12 sccm (right) of xenon flow and select discharge currents.

6.2   Characterization of the 2-cm-dia. cathode

The primary objective of this study is to investigate and reduce energetic ion production in the discharge plume of the 2-cm-dia. LaB_6 hollow cathode by directly injecting cold neutral gas into the cathode plume. Parameters varied in the study include the flow splits between the

internal and external cathode flows, the number of external gas injection sites, the locations of these injection sites, and the orifice size of the injectors for discharge currents of up to 250 A.

The parameter space under study is in list form for clarity:

Cathode flow rate: 10 to 20 sccm

The 2-cm-dia. cathode has a nominal flow operation of around 16 sccm without external flow. The 10 to 20 sccm range was selected to determine the trend for optimal cathode operation with external flow. The lower limit was selected to ensure that there was sufficient gas flow to support the large diameter cathode discharge. Increasing cathode flow reduces LaB_6 insert life by reducing the plasma contact area with the insert, and so a maximum limit of 20 sccm was chosen somewhat arbitrarily on this basis.

Injection flow rate: 0 to 20 sccm

The combined flow split of the internal and external flows was limited to 40 sccm to not overload the pumping system in the vacuum facility. Additionally, it was desired to maintain consistency in external flow amounts considered between all the cases studied, thus yielding a maximum external flow of 20 sccm. The baseline situation of no external injection (0 sccm) was used to compare and quantify the effects of external injection.

Discharge current: 25 to 250 A

The lower limit was selected to ensure that the cathode self-heating was sufficient to operate the discharge supply. Although the discharge power supply was capable of producing 300 A of current, an upper limit of 250 A was selected as to not cause the cathode to operate at high current conditions that could melt the cathode parts and cause cathode failure.

Injectors used: ring injector with point sources and jet injectors

See below for the motivation and description of these two types of injectors.

Injector locations

Injection sites were chosen to correspond to axial locations just upstream, on, and just downstream of the characteristic plasma spot or "ball" in the discharge plasma [9], while considering physical constraints of the experimental setup like the anode and solenoid placements. These axial locations were estimated with the system up to air and kept consistent for the entirety of the study.

Two types of external injection methods are utilized: point source injection, accomplished through a ring injector, and jet injection. The injectors are placed downstream of the cathode, between the anode and keeper face, at various axial distances. Photographs of the experimental setup with a ring injector or the dual-jet injectors are provided in Figure 18 and Figure 19, respectively. In the pictures, the surface seen behind the ring or jet injectors is coated by tungsten sputtered from the interior of the anode during energetic ion generation. The thick films tend to flake off when exposed to air, and so this surface is periodically cleaned to ensure that flakes do not occur during testing.
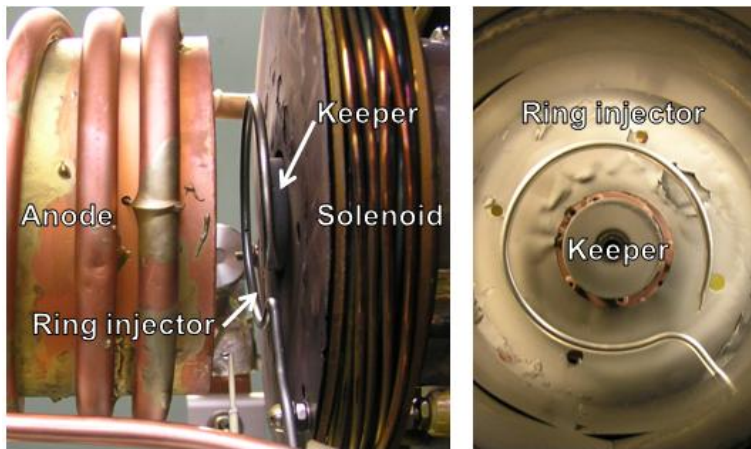

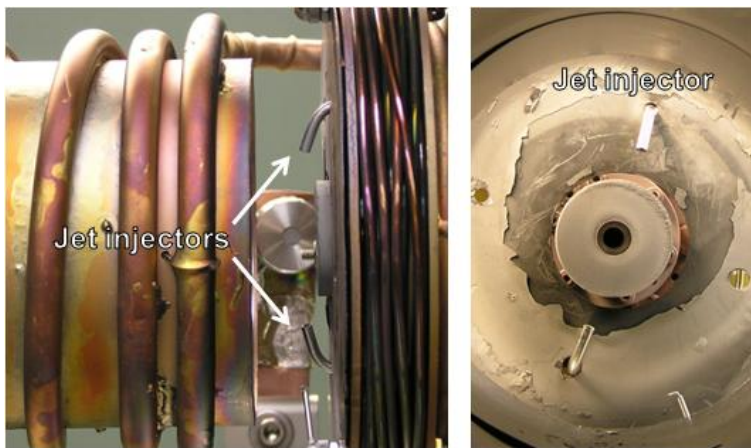**Figure 18: Experimental setup with a ring injector.**

Figure 19: Experimental setup with two jet injectors.

The point source injection method was accomplished by drilling several 1-mm-diameter holes into a 1/8"-dia. hollow stainless steel tube and then carefully bending the tubing into a circle as shown in Figure 18. The idea behind this design was to provide uniform gas injection into the plume because the gas leaves the orifices in relatively non-directional, uncollimated paths due to the small diameter of the orifices and the lack of steering of the gas by the ring geometry. For these reasons, we assume that each orifice in the ring injector behaves as a nearly hemispherical point source for neutral gas as illustrated by the upper schematic in Figure 20.

The jet injector, on the other hand, provides a direct stream of neutral gas into the plume region as illustrated in the lower schematic of Figure 20. This jet injector is formed by bending a 1/8"-dia. stainless steel hollow tube, the same kind as that used for the ring injector, into an obtuse L-shape as illustrated in Figure 19. Unlike the ring injector, all the gas that is injected into the feed end is released through a single orifice at the other end of the tube, and the injected gas has approximately a jet form.
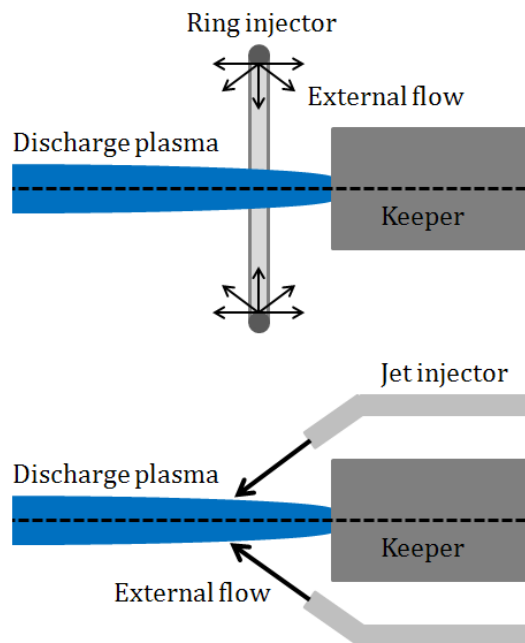
Figure 20: Schematic of injection flow paths for the ring (top) and jet (bottom) injectors.

Three basic types of injector schemes were investigated. Photographed in Figure 21, they are a ring injector of diameter   and with   injection holes, an arrangement of four jet injectors spaced at 90 degree increments with opposite injector orifices at a planar distance   , and an arrangement of two jet injectors oriented 180 degrees from each other with a planar distance   . Note that two ring diameters were considered in this study, one of diameter 2" and 7 injection holes and another of diameter 2.5" and 4 injection holes. Again, the flaky surface behind the injectors is from anode sputtering, which flakes when exposed to air and is periodically cleaned.
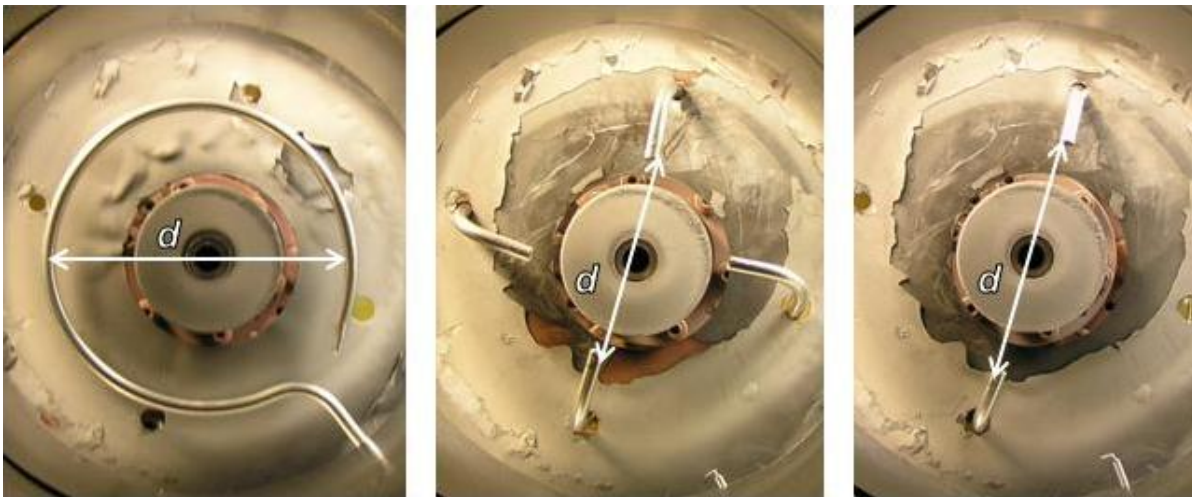
Figure 21: Photographs of the ring (left), 4-jet (middle), and 2-jet (right) injection schemes.

Table 2 tabulates the cases studied and the relevant details of each case. For the ring injectors, the "injector distance from the keeper" distance   is defined as the axial distance between the injection orifices in the ring and the keeper electrode orifice plate. For the jet injectors, the "injector distance from the keeper" distance   is the axial distance from the keeper orifice to the point at which the externally injected flow crosses the cathode/plume axis. For clarity, Figure 22 provides sketches of how this distance is defined for the ring and jet injectors.
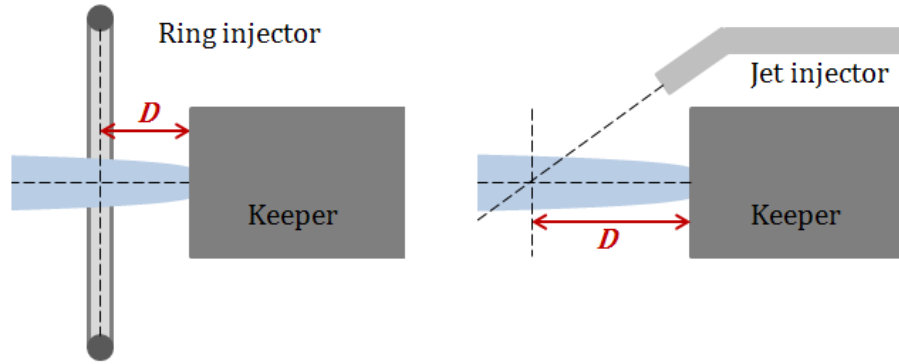
Figure 22: Schematic of the injector distance from the keeper for ring (left) and jet (right) injectors.

Table 2: Cases studied for the 2-cm-dia. LaB6 hollow cathode.

Case	Injector Specifications	Injector distance from keeper,	Cathode Flow	External Flow
1	- 2.5" dia. ring injector - 4 injection holes	0.3 cm	10 to 20 sccm	0 to 20 sccm
2	- 2.5" dia. ring injector - 4 injection holes	1.5 cm		
3	- 2" dia. ring injector - 7 injection holes	1.5 cm		
4	- 2" dia. ring injector - 7 injection holes	0.3 cm		
5	- 2 jet injectors - Orifices 1.6" apart	1.5 cm	10 , 16 sccm	
6	- 4 jet injectors - Orifices 1.6" apart	1.5 cm		
7	- 2 jet injectors - Orifices 2" apart	1.5 cm		
8	- 2 jet injectors - Orifices 2" apart	0.3 cm		
9	- 2 jet injectors - Orifices 2" apart	2.5 cm		

An RPA and flat probe are used to make ion energy distribution and ion flux measurements in the plume region for the various cases of interest. This data is then processed and analyzed for select flow split conditions described in Section 7.1 to yield erosion rates and projected lifetimes of the keeper face due to ion bombardment.

Before reporting results for the cases listed above, sample *I-V* and ion energy distribution curves obtained from an RPA trace are provided in Figure 23 to illustrate and define some of the parameters in the trace that are relevant to this study. Here, the "voltage at the maximum ion energy" is defined as the discriminator voltage at which the ion energy distribution reaches its maximum value. The "voltage spread at half the maximum ion energy" is the full-width (in voltage) of the ion energy distribution at half the maximum ion energy value (FWHM).
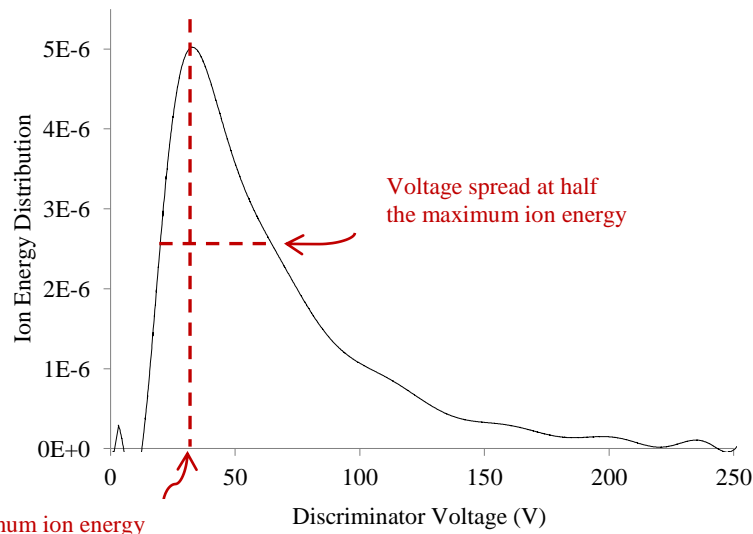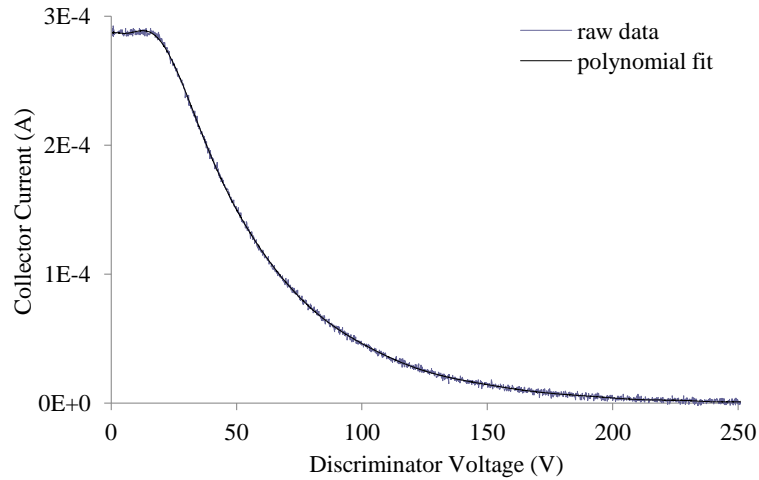
Figure 23: Sample current-voltage plot (top) and ion energy distribution curve (bottom) from RPA data.

In both vacuum facilities, the discharge power supplies are current controlled. When the discharge current is changed, the discharge voltage is allowed to stabilize before probe data is collected. This occurs on time scales of several minutes associated with the self-heating of the cathode as the discharge conditions are changed. Additionally, the discharge power supply in the JPL high current test facility could only provide discharge currents for the cases where the corresponding discharge voltage was 30 V or less. This determined the maximum discharge

currents that could be achieved for the cases considered up to the maximum 250 A that the cathode could be safely operated at.

Case 1 Results:

To determine the effects of neutral gas injection into the hollow cathode plume on the energetic ion production, a large array of RPA and flat probe data was first collected for Cases 1 to 4, and then a narrower parameter space was studied in more detail to accommodate the time constraints of the thesis project. For each of these cases, the ion energy distribution was measured for cathode flows of 10, 12, 14, 16, 18, 20 sccm, for external flows of 0, 5, 10, 15, 20 sccm, and for discharge currents of 25, 50, 75, 100, 125, 150, 175, 200, 225, 250 A. After processing the data for these cases, it was apparent that the same general profile was exhibited for the ion energy vs. cathode flow vs. external flow relationship for all four cases of the injector geometry as well as for each of the discharge currents considered. For this reason, two sets of data from Case 1 are presented here to represent and highlight the overall effect of external gas injection on the production of energetic ions in the cathode discharge plume. Specifically, these sets are for discharge current operation of 25 A and 75 A.

Figure 24 to Figure 27 provide three dimensional plots of select parameters of the ion energy distribution as functions of the cathode and external flows for discharge currents of 25 A and 75 A, respectively. In Figure 24 and Figure 26, the voltage at the maximum ion energy is plotted against the two flows while in Figure 25 and Figure 27, the voltage spread at half the maximum ion energy is plotted against these same flows. For both discharge currents, reducing cathode flow while keeping external flow constant increased energetic ion production in the plume. In contrast, increasing external flow for constant cathode flow was observed to reduce the energetic ion production. The greatest reduction of energetic ion production occurred when

37

both the internal and external flows were at the maximum value. Analogously, the worst performance in terms of high energy ion production was exhibited for the combination of high discharge current and no external xenon injection. It should be noted that while maxing out on cathode flow reduces energetic ion production in the plume, high cathode flow pushes the plasma density peak inside the cathode toward the orifice (as shown in Section 6.1), thereby reducing the contact area between the xenon gas and LaB_6 surface and reducing insert life.

The voltage at the maximum ion energy and the voltage spread at half the maximum of the ion energy exhibit the same trends: as the voltage at maximum ion energy increases with increased cathode flow and/or decreased external flow, so does the width of the energy spread. Similarly, as the voltage at maximum ion energy decreases with decreasing cathode flow and/or increasing external flow, so does the width of the energy spread.
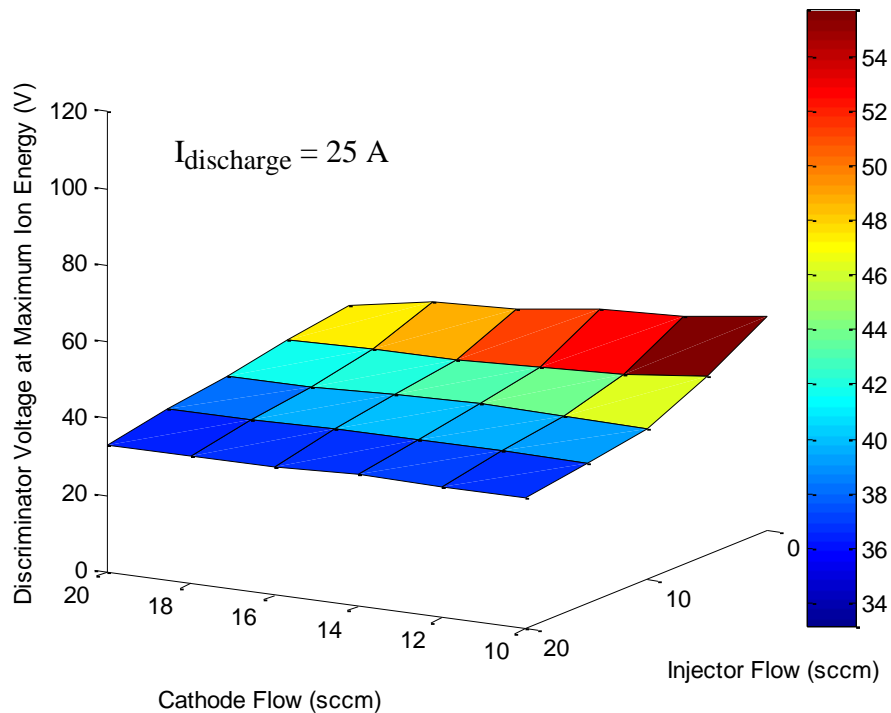
Figure 24: Discriminator voltage at maximum ion energy plotted against cathode flow and injector flow at 25 A for the 2-cm-dia. cathode.
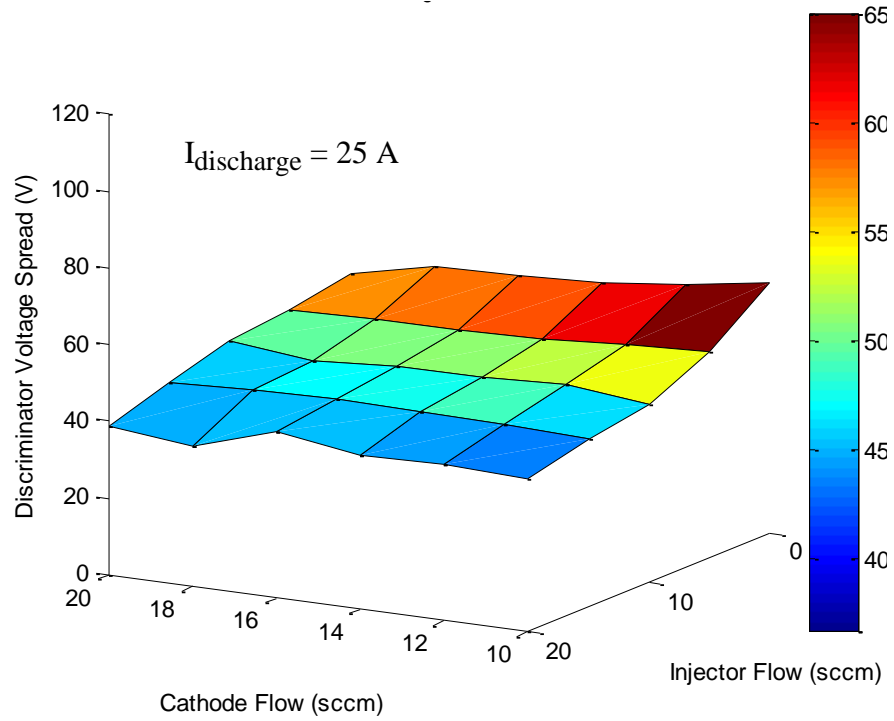
Figure 25: Discriminator voltage spread at half the maximum ion energy plotted against the cathode and injector flows at 25 A for the 2-cm-dia. cathode.
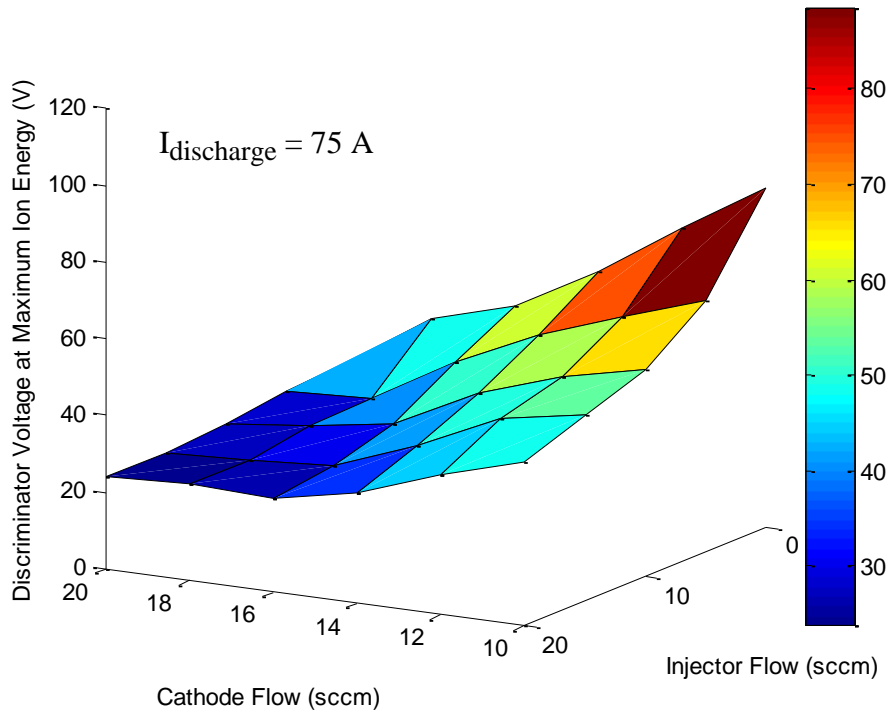
Figure 26: Discriminator voltage at maximum ion energy plotted against cathode flow and injector flow at 75 A for the 2-cm-dia. cathode.
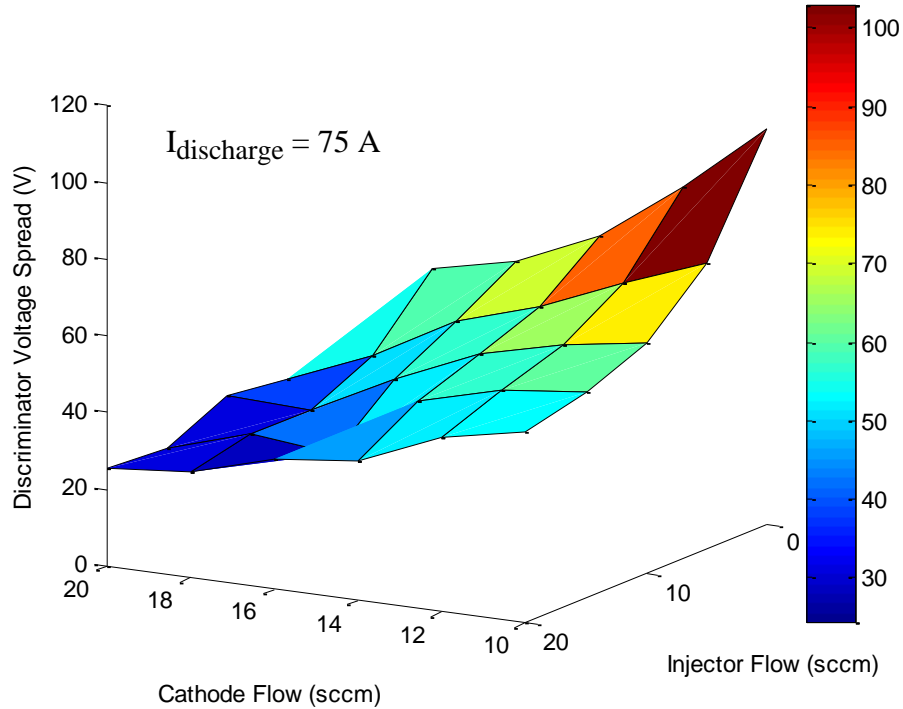
Figure 27: Discriminator voltage spread at half the maximum ion energy plotted against the cathode and injector flows at 75 A for the 2-cm-dia. cathode.

To determine the effects of discharge current on energetic ion production, plots of the ion energy against the discharge current for external flows of 0 to 20 sccm are presented for cathode flow rates of 10 sccm in Figure 28 and 16 sccm in Figure 29. For both low cathode flow (10 sccm) operation and high cathode flow (16 sccm) operation, the two sets of data reveal consistent trends as discharge current or external flow is increased. Increasing discharge current increases the ion energy; both the voltage at the maximum ion energy and the voltage spread at half the maximum ion energy increase. Introducing external flow reduces the ion energy, with more external flow corresponding to greater reduction in energetic ion production. However at lower discharge current, the ion energy values seem to converge slightly for all external flows; the divergence between external flows increases with increasing discharge current. For example, at 10 sccm of cathode flow, the difference in the voltage at the maximum ion energy between 0 sccm of external flow and 20 sccm of external flow increases from 20 V at 25 A of discharge

current to 43 V at 75 A of discharge current. Similarly, for the 16 sccm cathode case, this difference increases from 10 V at 25 A to about 47 A at 175 A. These same trends are observed in the energy spread value at half the maximum ion energy (the FWHM). It should be noted that there is a general minimum in the ion energy profiles for the 16 sccm cathode flow case at discharge currents below 100 A. Above 75 A, the ion energy increases with decreasing discharge current.
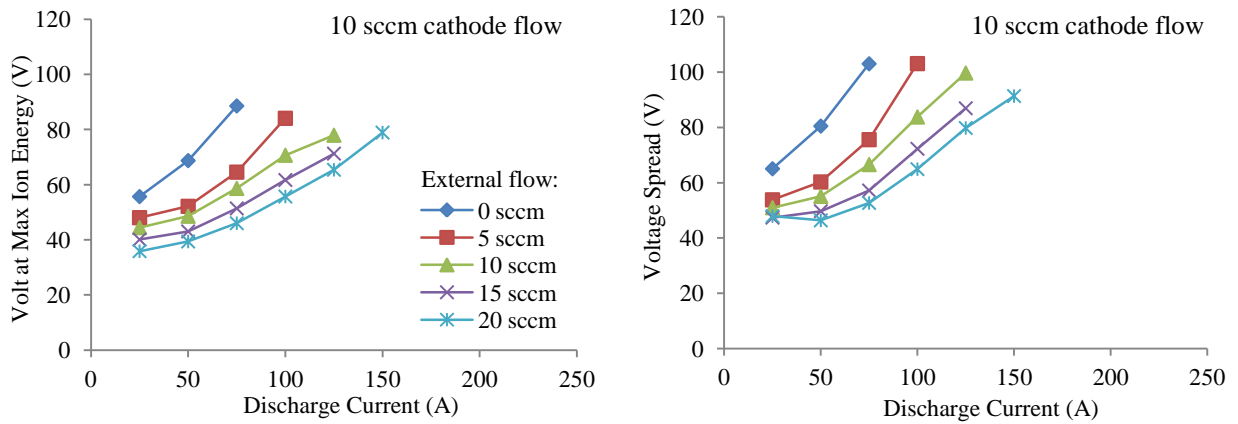
Figure 28: Discriminator voltage at maximum ion energy (left) and discriminator voltage spread at half the maximum ion energy (right) plotted against cathode flow and injector flow for 10 sccm cathode flow.
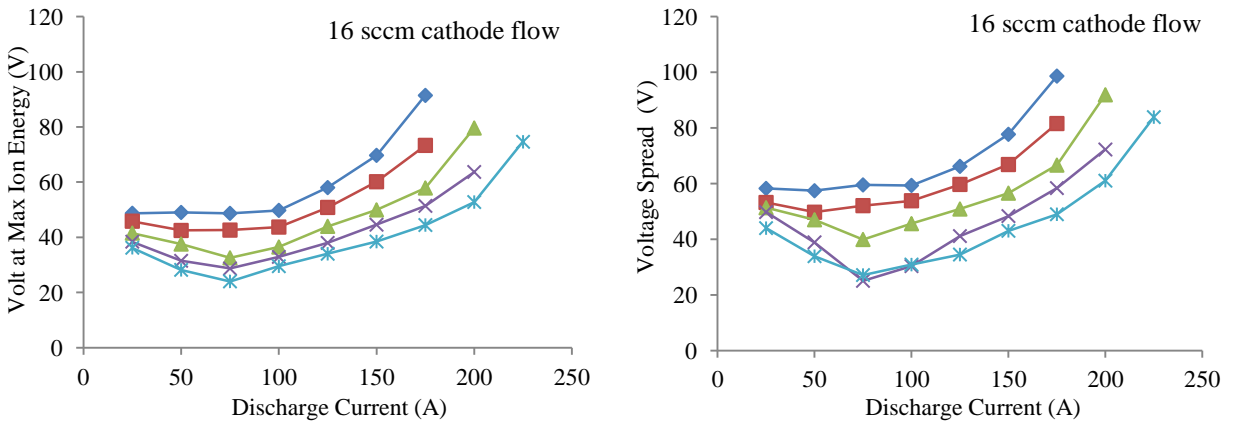
Figure 29: Discriminator voltage at maximum ion energy (left) and discriminator voltage spread at half the maximum ion energy (right) plotted against cathode flow and injector flow for 16 sccm cathode flow.

It is interesting to note that the ion energy and discharge voltage have the same general profiles when plotted against the discharge current, with their minimum values occurring at roughly the same discharge currents. Figure 30 plots discharge voltage against discharge current for the 10 sccm and 16 sccm cathode flow situations of Case 1. As explained in the previous section, the cathode operates in plume mode at lower discharge currents and transitions to jet mode operation at higher currents.
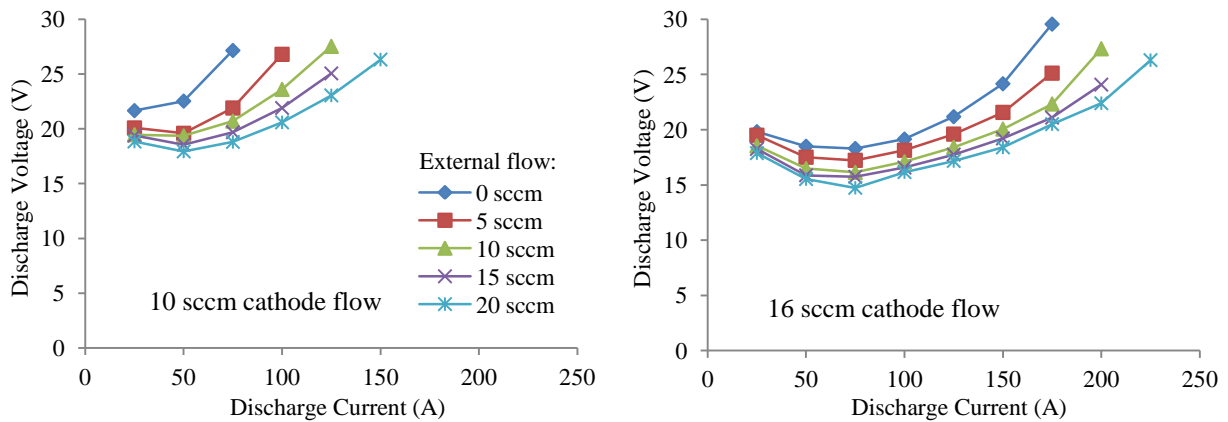
Figure 30: Discharge voltage vs. discharge current for 10 sccm (left) and 16 sccm (right) cathode flow.

Cases 1-7 Results:

To determine the injector scheme that provides the greatest reduction in energetic ion production in the cathode plume, this section reports the results from Cases 1 to 7 for cathode flow rates of 10 sccm and 16 sccm. The injector type and experimental setup for each case can be found in Table 2. Figure 31 provides plots of the voltage at maximum ion energy against the discharge current for the injector configurations found in Cases 1 to 7 and for no external flow for reference. The upper four plots are for 10 sccm cathode flow and 5 sccm, 10 sccm, 15 sccm, and 20 sccm of external flows. The lower four plots are for 16 sccm cathode flow and 5 sccm, 10 sccm, 15 sccm, and 20 sccm of external flows. It is apparent that injecting neutral gas into the

plume region, regardless of the type of injector or location of the injectors, decreases the production of high energy ions for all situations studied here. In fact, for some situations external gas injection reduces the maximum ion energy by over 50% compared to no external injection. Although external injection reduces energetic ion production in the plume regardless of injection type and injection location, Figure 31 reveals that both the 2.5" diameter and 2" diameter ring injectors performed similarly in reducing energetic ion production regardless of injector size and location for 10 sccm and 16 sccm cathode flow. Further, both jet injector schemes preformed better than the ring injectors by up to several tens of voltages for the discharge currents and cathode flows considered. Additionally, the plots show that the energetic ion reduction performance from the 2-jet-injection arrangement and the 4-jet-injection arrangement are similar to one another.

Ion energy plots for cathode flows of 10 - 20 sccm and external flows 0 - 20 sccm for Cases 1 - 4 and select flow splits for Cases 5 and 6 are provided in the appendix for completeness and to further support the findings that (1) external injection reduces energetic ion production with greater performance gains for more external flow, (2) the ring injectors displayed comparable performance to one another regardless of size and location, (3) the jet injectors outperformed the ring injectors for the same external flow amounts by a couple to tens of voltages, and (4) the two-jet-injector arrangement performed similarly to the four-jet-injector arrangement.
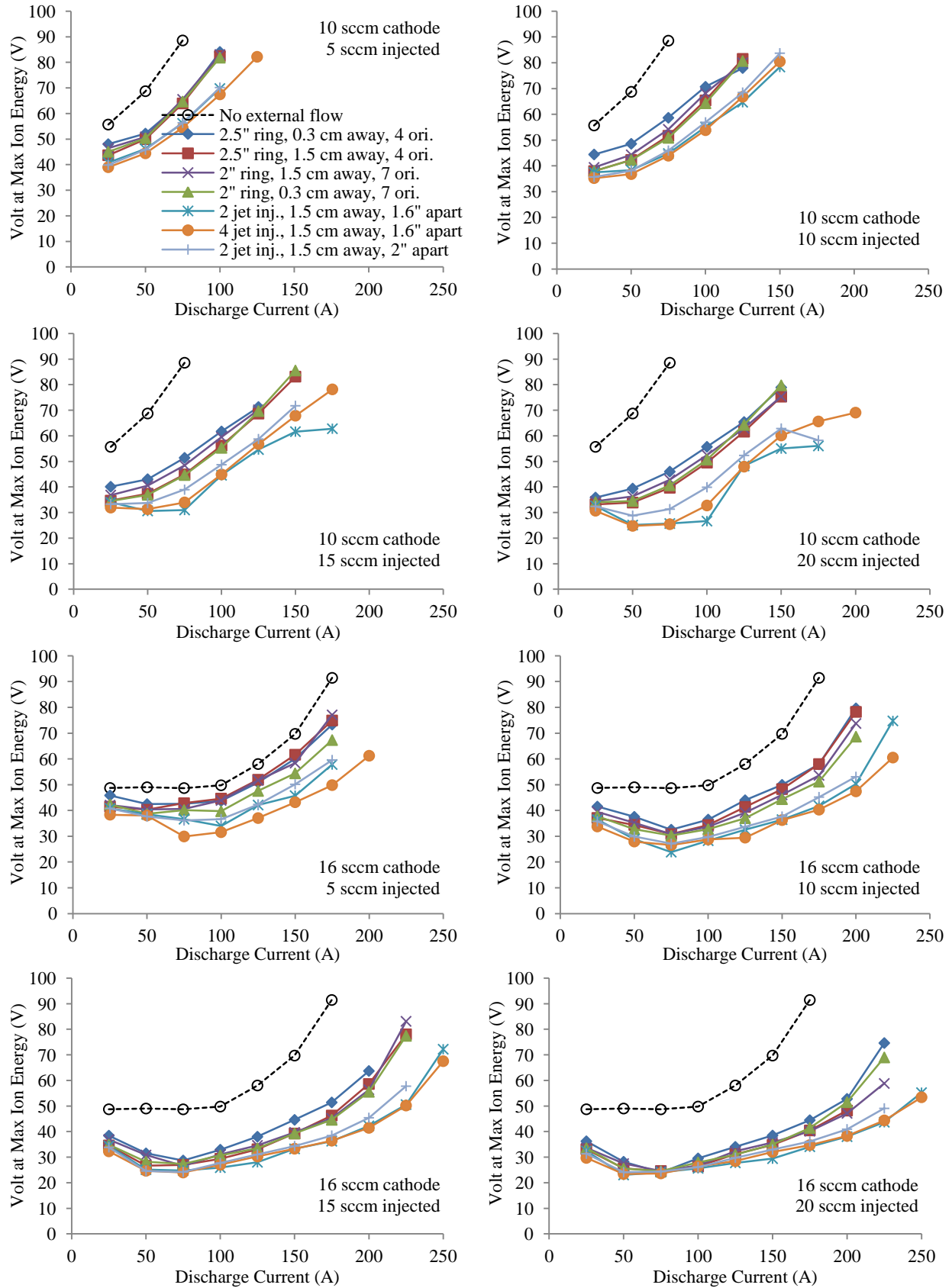
Figure 31: Ion energy plotted against discharge current for Cases 1 to 7 for various flow splits.

Cases 7-9 Results:

Upon discovering that jet injection provided greater energetic ion reduction in the cathode plume than point injection by the ring injectors, Cases 7 - 9 were investigated to determine the effects of jet injector axial location on the production of energetic ions. The performance observed between the four injectors and two injector cases was very similar. Additionally, the two-jet injector scheme is easier to fabricate and install because of fewer parts and would be easier to incorporate into an EP thruster system. For these reasons, further external injections studies were focused on the two injector jet case.

In Figure 32, the voltage at maximum ion energy is plotted against discharge current for 10 sccm and 16 sccm cathode flows for Cases 7 - 9 and no external flow for reference. The upper four plots are for 10 sccm cathode flow and 5 sccm, 10 sccm, 15 sccm, and 20 sccm of external flows. The lower four plots are for 16 sccm cathode flow and 5 sccm, 10 sccm, 15 sccm, and 20 sccm of external flows. The injectors are spaced 2" apart and placed at axial locations of 0.3 cm (just upstream of the characteristic plasma spot in the discharge plume), 1.5 cm (at the plasma spot), and 2.5 cm (just downstream of the plasma spot). The plots in Figure 32 reveal that the two-jet injector scheme offers similar reductions in energetic ion production regardless of whether the injectors are placed just upstream of the plasma spot, at the plasma spot, and just downstream of the plasma spot. This suggests that injection of gas directly into the near-cathode plume is effective in reducing the energetic ion production rate, irregardless of precisely where the injection occurs.
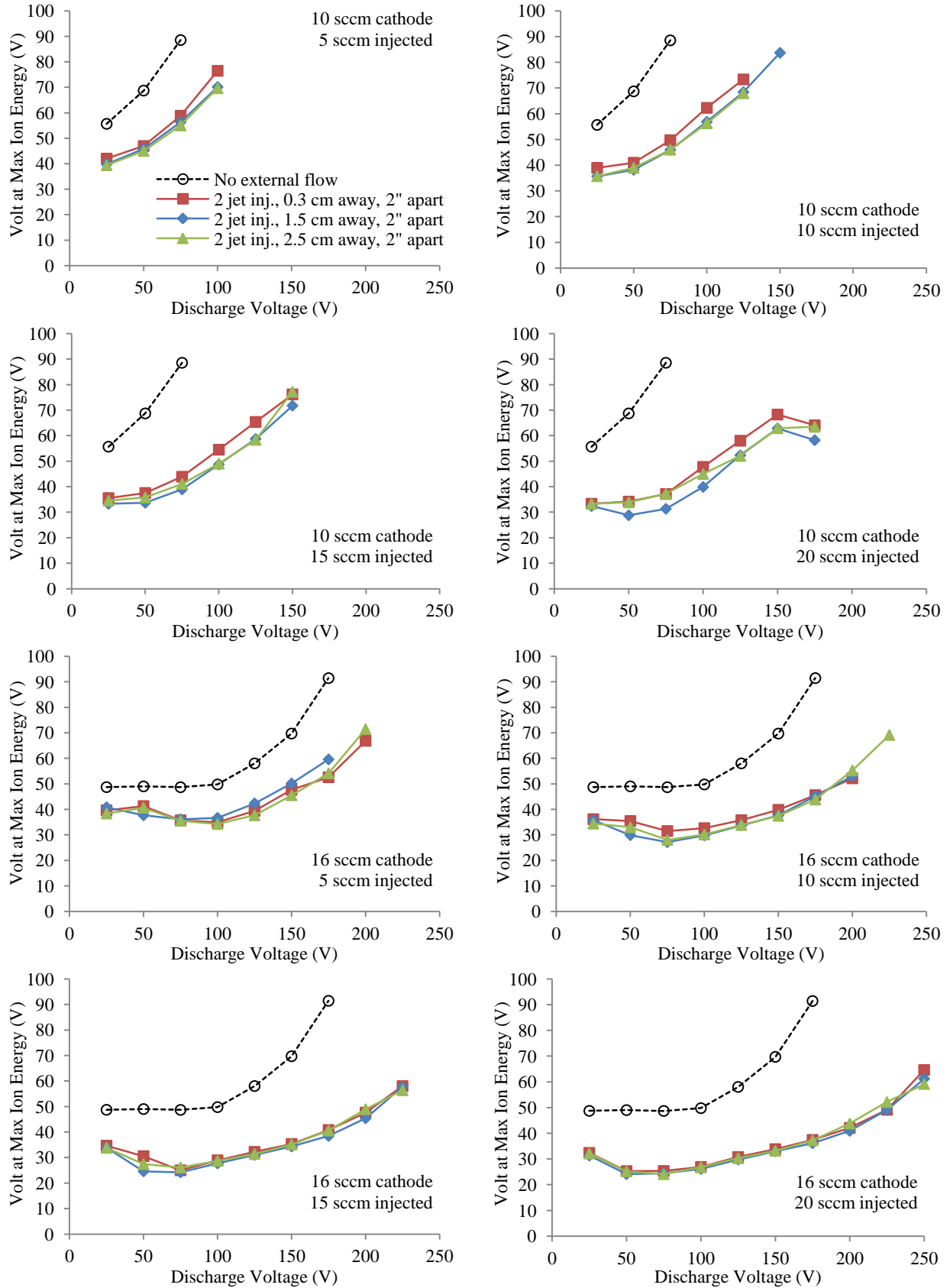
Figure 32: Ion energy plotted against discharge current for Cases 7 to 9 for various flow splits.

7 Analysis and Discussion

7.1 Sputter Rates and Cathode Life

The impact of the energetic ion generation on the cathode life can be shown by evaluating the lifetime of the cathode and keeper surfaces due to sputter-erosion by ion bombardment. The energy of the ions is determined from the ion collector current versus discriminator voltage of the RPA. The rate R per unit area at which atoms are removed from the surface being bombarded [9] is given by

$$R = \int_0^{V_o} \frac{I(V)Y(V)}{eA_p} dV = \frac{1}{e} \int_0^{V_o} J(V)Y(V)dV \left[\frac{\text{atoms}}{\text{cm}^2 \cdot \text{s}}\right] \tag{6}$$

where $I(V)$ is the ion current to the surface as a function of the energy of the ions, $Y(V)$ is the energy dependent sputtering yield of the surface, e is the electronic charge, A_p is the area, V is the ion energy, V_o is the discriminator voltage at which the collected ion current goes to zero, and $J(V)$ is the ion current density to the surface as a function of the ion energy. The erosion rate of the surface E_r is given by

$$E_r = \frac{RW}{\rho A_v} = \frac{W \int_0^{V_o} J(V)Y(V)dV}{e\rho A_v} \left[\frac{\text{cm}}{\text{s}}\right] \tag{7}$$

where ρ is the density of the material, A_v is Avogadro's number, and W is the atomic weight of the material being sputtered. The time it takes for the ion flux to erode through a thickness d of the surface is

$$E_r = \frac{RW}{\rho A_v} = \frac{W \int_0^{V_o} J(V)Y(V)dV}{e\rho A_v} \left[\frac{\text{cm}}{\text{s}}\right] \tag{8}$$

The ion energy analyzer current data is multiplied against the sputtering yield [38] and integrated over the discrimination grid voltage to obtain the surface erosion rate from Equation

(6. This sputtering rate is used to calculate the life of the keeper electrode using Equation (8 for molybdenum and carbon keepers assuming that the keeper fails after the 0.15-mm-thick keeper face has eroded through. Data from the NSTAR ion thruster life test showed that a combination of keeper face and keeper orifice erosion sputtered the keeper away, but the contribution of orifice diameter erosion in these high current cathodes could not be addressed in this work.

The RPA data, taken radially away from the cathode plume, is used to calculate the sputtering rate normalized to the ion flux to the keeper face by using flat probe data taken at the RPA location and at the face of the keeper. It is assumed in this calculation that the ion energy distribution is the same radially from the plume and axially upstream toward the keeper. While this might not be the case, the general trends associated with plume gas injection for different discharge currents and cathode flow rates are likely indicative of the relative sputtering rates and keeper surface lifetimes.

Data for several discharge current and gas injection flow cases are shown in Figure 33 and Figure 34. Operation at high discharge current and low cathode gas flow produces very energetic ions, which results in keeper lifetimes of less than 5000 hours. With sufficient cathode gas flow and injected flow rates, the keeper life can be extended to over 10,000 hours at discharge currents of up to 200 A. Higher discharge currents will require either more cathode flow or more injected flow, which could not be tested in the current facility due to pumping speed limitations.
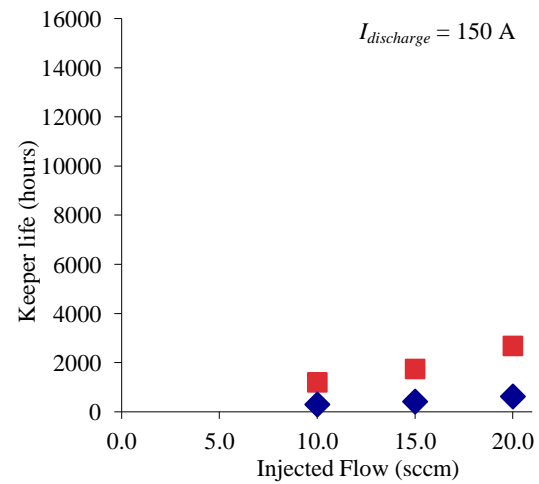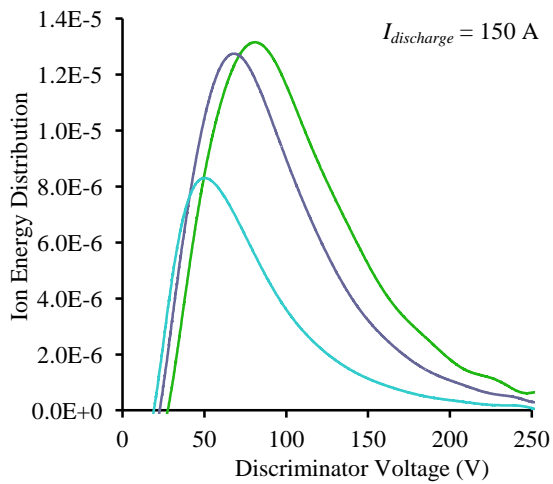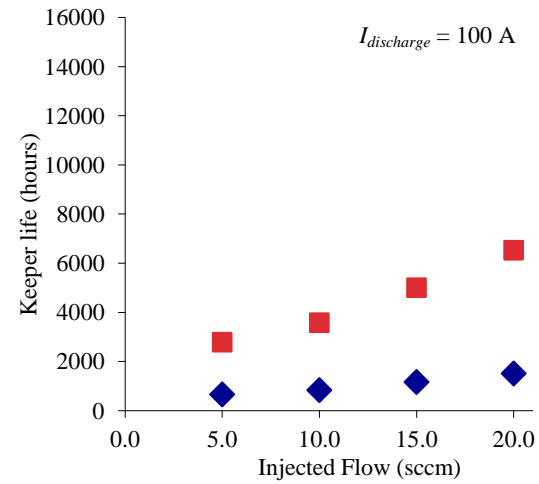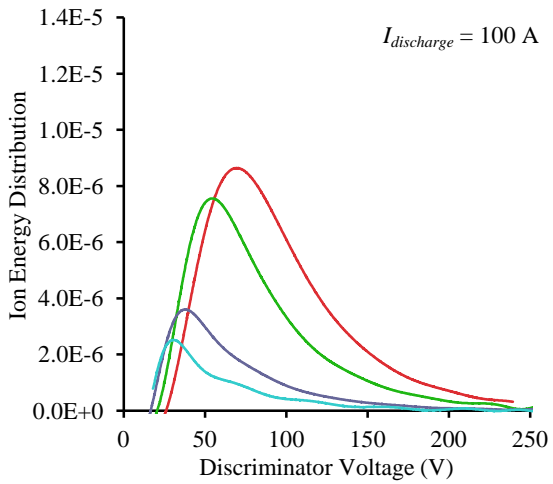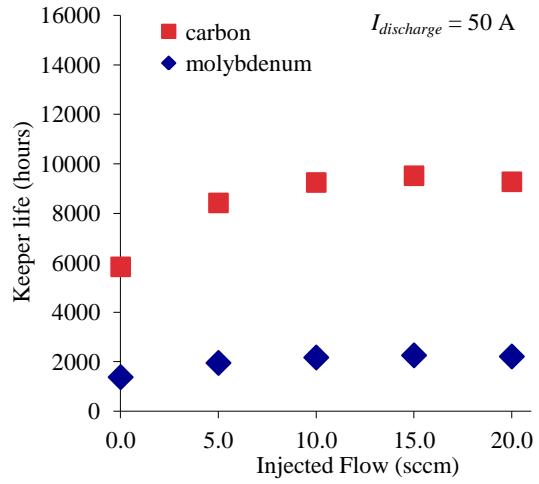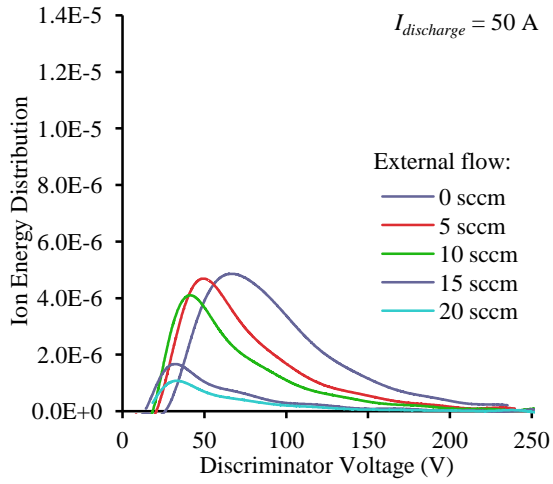
Figure 33: Ion energy distribution vs discriminator voltage (top row) and keeper life vs external flow (bottom row) for 10 sccm of cathode flow and at 50 A (left column), 100 A (middle column), and 150 A (right column) of discharge current.
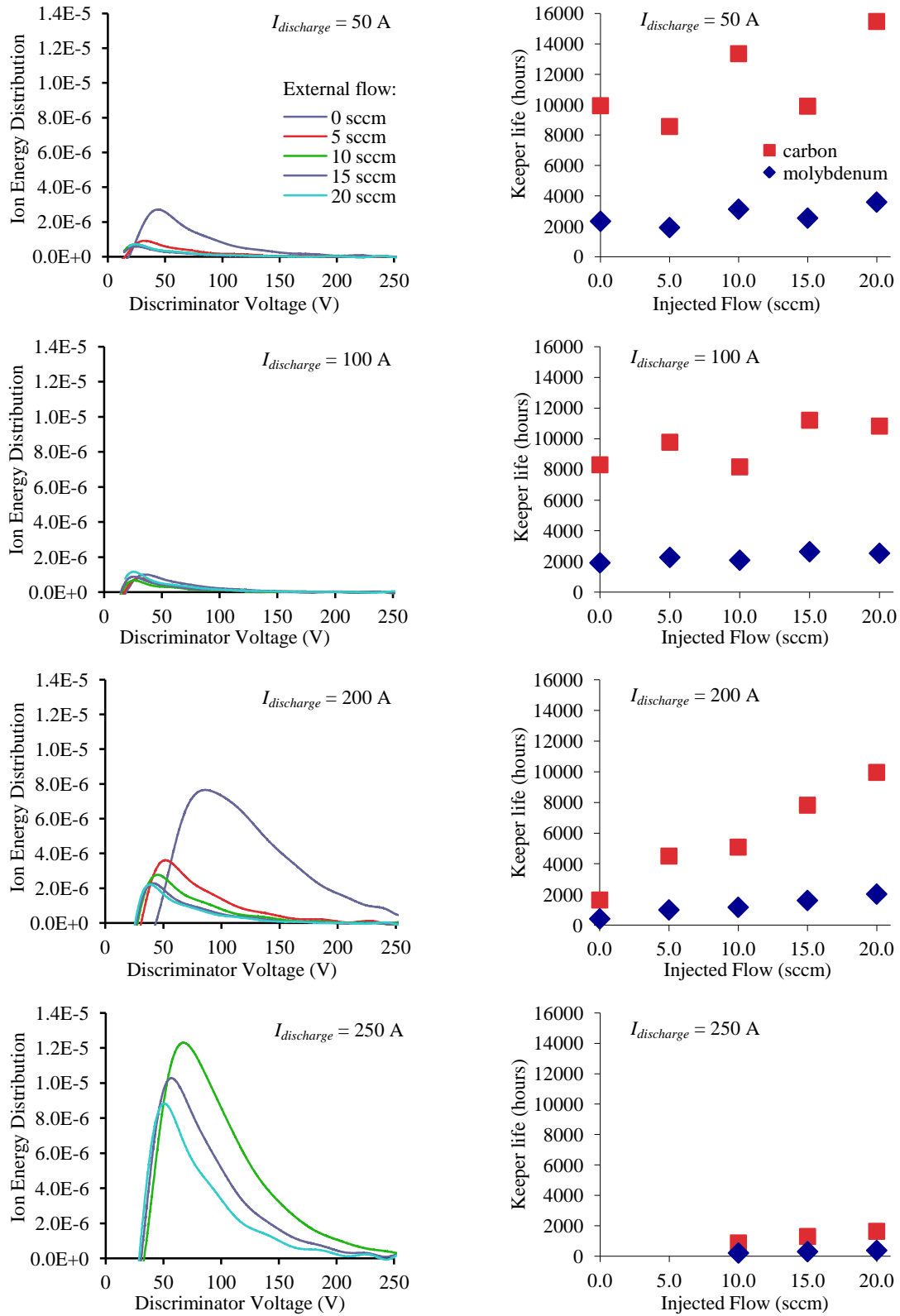
Figure 34: Ion energy distribution vs discriminator voltage (top row) and keeper life vs external flow (bottom row) for 16 sccm of cathode flow and at 50 A (1st column), 100 A (2nd column), 200 A (3rd column), and 250 A (4th column) of discharge current.

7.2   Considerations in discharge voltage, flow splits, and injection type

In general, higher cathode and external flows is observed to lower the discharge voltage, which in turn is correlated to lower energetic ion production. In the situation where the hollow cathode gets into the mechanism that produces energetic ions from plasma potential fluctuations, then this discharge voltage dependence is just a DC off set for the rf potentials [28]; the total ion energy responsible for sputter-induced damage is the sum of the DC discharge voltage level and the rf plasma potential to get the total ion energy that does the damage.

Results in the Chapter 6 indicate that the energetic ion production in the cathode plume is at a minimum when both internal cathode flow and external gas injection are at their maximum values. This is true for all discharge currents studied. However, while there are reductions in energetic ion production for increased cathode flow, high cathode flow also pushes the plasma density peak toward the orifice which reduces the plasma contact area with the LaB_6 surface and reduces the LaB_6 insert life. As a possible compromise to this problem, the cathode can be operated at the highest internal flow rate that will still yield long insert life while as much external flow is injected into the plume region as the system can handle in terms of propellant costs and specific impulse requirements of the mission to reduce energetic ion production.

As shown in Figure 31, jet injection was demonstrated to be more effective than point injection at reducing energetic ion production in the discharge plume. This may be due to the fact that in jet injection, nearly all the neutral gas is injected directly into the plasma discharge and so there is more interaction between the plasma and the neutrals, whereas in the un-collimated point injection, a large fraction of the gas likely misses the discharge plume and the distributed cloud of neutrals in and around the plume region is less effective for producing collisions and ionization that reduce the energetic ion production than the jet streams.

8   Conclusion

This work has demonstrated that external injection of neutral gas directly into the discharge plume can drastically reduce the production of high-energy ions that are responsible for keeper erosion that ultimately limits cathode life and leads to cathode failure. Keeper electrode life can be increased from under 2,000 hours at low cathode flow rates and no external injection to over 10,000 hours at higher cathode and external flows at up to 200 A. While this is likely sufficient for development of the high power Hall thrusters in the laboratory and for the first generation of mission applications of these high current EP systems, the following generation of EP missions will likely require hollow cathodes with lifetimes of over 10 years. More investigations aimed at suppressing the energetic ion production, coupled with detailed modeling efforts, are needed to further understand the mechanisms that are responsible for energetic ion production in the plume. This work will be required to develop and produce the next generation of long life, high current hollow cathodes.

9   Bibliography

[1] K. Nishiyama, S. Hosoda, H. Koizumi, Y. Shimizy, I. Funaki, H. Kuninaka, M. Bodendorfer, J. Kawaguchi and D. Nakata, "Hayabusa's Way Back to Earth by Microwave Discharge Ion Engines," in *AIAA-2010-6862, 47th AIAA Joint Propulsion Conference*, San Diego, California , 2011.

[2] C. Koppel, M. Cramayel, F. Marchandise, M. Prioul, D. Estuglier and F. Darnon, "The Smart-1 Electric Propulsion Subsystem Around the Moon: In Flight Experience," in *AIAA-2005-3671, 41st AIAA Joint Propulsion Conference and Exhibit*, Tucson, Arizona, July 10-13.

[3] C. Garner, M. Rayman and J. Brophy, "In-Flight Operation of the Dawn Ion Propulsion System: Status at One Year From the Vesta Rendezvous," in *AIAA-2010-7111, 47th AIAA Joint Propulsion Conference*, San Diego, California, July 31-3, 2011.

[4] J. Brophy, "Asteroid Return Mission Feasibility Study," in *AIAA-2011-5665, 47th AIAA Joint Propulsion Conference*, San Diego, California, July 31-3, 2011.

[5] J. Brophy, R. Gershman, N. Strange, D. Landau, R. Merrill and T. Kerslake, "300-kW Solar Electric Propulsion System Configuration for Human Exploration of Near-Earth Asteroids," in *AIAA-2011-551, 47th AIAA Joint Propulsion Conference*, San Diego, California, July 31-3, 2011.

[6] N. Strange, R. Merrill, D. Landau, B. Drake, J. Brophy and R. Hofer, "Human Missions to Phobos and Deimos Using Combined Chemical and Solar Electric Propulsion," in *AIAA-2011-5663, 47th AIAA Joint Propulsion Conference*, San Diego, California, July 31-3, 2011.

[7] D. Goebel, K. Jameson, I. Katz and I. Mikellides, "Energetic ion production and keeper erosion in hollow cathode discharges," in *IEPC 2005-266, International Electric Propulsion Conference*, Princeton, NJ, Oct. 31st - Nov. 4th, 2005.

[8] D. Goebel, K. Jameson, I. Katz and I. Mikellides, "Plasma potential behavior and plume mode transitions in hollow cathode discharges," in *IEPC 2007-277, International Electric Propulsion Conference*, Florence, Italy, Sept. 17-20, 2007.

[9] D. Goebel and I. Katz, Fundamentals of Electric Propulsion, Hoboken, New Jersey: John Wiley & Sons, Inc., 2008.

[10] J. Cronin, "Modern dispenser cathodes," *IEE Proceedings,* vol. 128, no. 1, pp. 19-32, 1981.

[11] B. Arkhopov and K. Kozubsky, "The development of the cathode compensators for stationary plasma thrusters in the USSR," in *IEPC 91-023, 22nd International Electric Propulsion Conference*, Viareggio, Italy, Oct. 14-17, 1991.

[12] V. Kim, "Electric propulsion activity in Russia," in *IEPC 2001-005, 27th International Electric Propulsion Conference*, Pasadena, California, Oct. 14-19, 2001.

[13] D. Goebel and R. Watkins, "LaB6 hollow cathodes for ion and hall thrusters," in *AIAA-2005-4239, 41st Joint Propulsion Conference*, Tucson, Arizona, July 11-13, 2005.

[14] D. Goebel, R. Watkins and K. Jameson, "LaB6 hollow cathodes for ion and Hall thrusters," *AIAA Journal of Propulsion and Power,* vol. 23, no. 3, pp. 527-528, 2007.

[15] D. Goebel and R. Watkins, "Compact lanthanum hexaboride hollow cathode," *Review of Scientific Instruments,* Vols. 81, 083504, 2010.

[16] J. Lafferty, "Boride cathodes," *Journal of Applied Physics ,* vol. 22, pp. 299-309, 1951.

[17] O. Richardson, "Electron theory of matter," *Philips Magazine,* vol. 23, pp. 594-627, 1912.

[18] A. Forrester, Large Ion Beams, New York: Wiley-Interscience, 1988.

[19] E. Storms and B. Mueller, "Storms and Mueller, "A study of surface stoichiometry and thermionic emission using LaB6," *Journal of Applied Physics,* vol. 50, pp. 3691-3698, 1979.

[20] J. Pelletier and C. Pomot, "Work function of sintered lanthanum hexaboride," *Applied Physics Letters,* vol. 34, pp. 249-251, 1979.

[21] W. Kohl, Handbook of Materials and Techniques for Vacuum Devices, New York: Reinhold Publishing Corporation, 1967.

[22] K.N.Leung, P. Pincosy and K. Ehlers, "Directly heated lanthanum hexaboride filaments," *Review of Science Instruments,* vol. 55, pp. 1064-1068, 1984.

[23] D. Goebel and E. Chu, "High current lanthanum hexaboride hollow cathodes for high power Hall thrusters," in *32nd International Electric Propulsion Conference*, Wiesbaden, Germany, September 11 – 15, 2011.

[24] D. Goebel, J. Crow and A. Forrester, "Lanthanum hexaboride hollow cathode for dense

plasma production," *Review of Scientific Instruments,* vol. 49, pp. 469-472, 1978.

[25] D. Goebel, Y. Hirooka and T. Sketchley, "Large area lanthanum hexaboride electron emitter," *Review of Scientific Instruments,* vol. 56, pp. 1717-1722, 1985.

[26] L. Favreau, "Cataphoretic Coating Lanthanum Boride on Rhenium Filaments," *Review of Scientific Instruments,* vol. 36, pp. 856-857, 1965.

[27] I. Kameyama and P. Wilbur, "Measurements of ions from high-current hollow cathodes using electrostatic energy analyzer," *Journal of Propulsion and Power,* vol. 16, p. 529, 2000.

[28] D. Goebel, K. Jameson, I. Katz and I. Mikellides, "Potential fluctuations and energetic ion production in hollow cathode discharges," *Physics of Plasma,* vol. 14, 2007.

[29] V. Friedly and P. Wilbur, "High current hollow cathode phenomena," *Journal of Propulsion and Power,* vol. 8, p. 635, 1992.

[30] I. Kameyama and P. Wilbur, "Potential-hill model of high-energy ion production near high current hollow cathodes," in *ISTS 98-a-2-17, 21st International Symposium on Space Technology and Science*, Sonic City, Omiya, Japan, May 1998.

[31] W. Tighe, K. Freick and K. Chien, "Performance evaluation and life test of the XIPS hollow cathode heater," in *AIAA_2005-4066, 41st Joint Propulsion Conference*, Tucson, Arizona, July 10-13, 2005.

[32] D. Goebel, K. Jameson, I. Katz and I. Mikellades, "Hollow Cathode Theory and Modeling: I. Plasma Characterization with Miniature Fast-Scanning Probes," *Journal of Applied Physics,* vol. 98, no. 11, 2005.

[33] L. King, "Transport-property and mass spectral measurements in the plasma exhaust plume of a Hall effect space propulsion system," Ph.D. Dissertation, Department of Aerospce Engineering, University of Michigan, Ann Arbor, Michigan, 1998.

[34] I. Hutchinson, Principles of Plasma Diagnostics, Cambridge: Cambridge University Press, 1987.

[35] F. Chen, Plasma Diagnostic Techniques, New York: Academic Press, 1965.

[36] K. Jameson, *Investigation of Hollow Cathode Effects on Total Thruster Efficiency in a 6 kW Hall Thruster, A PhD Dissertation,* University of California, Los Angeles, 2008.

[37] D. Goebel, K. Jameson, R. Watkins, I. Katz and I. Mikellides, "Hollow cathode theory and experiment. I. Plasma characterization using fast miniature scanning probes," *Journal of Applied Physics,* vol. 98, 2005.

[38] R. Kolasinski, J. Polk, D. Goebel and L. Johnson, "Carbon sputtering yield measurements at grazing incidence," *Applied Surface Science,* vol. 254, no. 8, 2008.

[39] E. Storms and B. Mueller, "Phase relationship, vaporization and thermodynamic properties of the lanthanum-boron system," *Journal of Chemical Physics,* vol. 82, pp. 51-59, 197.